

# MTH1 inhibition eradicates cancer by preventing sanitation of the dNTP pool

Helge Gad<sup>1\*</sup>, Tobias Koolmeister<sup>1\*</sup>, Ann-Sofie Jemth<sup>1\*</sup>, Saeed Eshtad<sup>1\*</sup>, Sylvain A. Jacques<sup>1\*</sup>, Cecilia E. Ström<sup>1\*</sup>, Linda M. Svensson<sup>2</sup>, Niklas Schultz<sup>1</sup>, Thomas Lundbäck<sup>1,3</sup>, Berglind Osk Einarsdottir<sup>4</sup>, Aljona Saleh<sup>5</sup>, Camilla Göktürk<sup>1</sup>, Pawel Baranczewski<sup>1,6</sup>, Richard Svensson<sup>3,6</sup>, Ronnie P.-A. Berntsson<sup>2</sup>, Robert Gustafsson<sup>2</sup>, Kia Strömberg<sup>1</sup>, Kumar Sanjiv<sup>1</sup>, Marie-Caroline Jacques-Cordonnier<sup>1</sup>, Matthieu Desroses<sup>1</sup>, Anna-Lena Gustavsson<sup>1,3</sup>, Roger Olofsson<sup>4</sup>, Fredrik Johansson<sup>7</sup>, Evert J. Homan<sup>1</sup>, Olga Loseva<sup>1</sup>, Lars Bräutigam<sup>1</sup>, Lars Johansson<sup>1,3</sup>, Andreas Höglund<sup>1</sup>, Anna Hagenkort<sup>1</sup>, Therese Pham<sup>1</sup>, Mikael Altun<sup>1</sup>, Fabienne Z. Gaugaz<sup>1,6</sup>, Svante Vikingsson<sup>1,8</sup>, Bastiaan Evers<sup>1,†</sup>, Martin Henriksson<sup>1</sup>, Karl S. A. Vallin<sup>1</sup>, Olov A. Wallner<sup>1</sup>, Lars G. J. Hammarström<sup>1,3</sup>, Elisee Wiita<sup>1</sup>, Ingrid Almlöf<sup>1</sup>, Christina Kalderén<sup>1</sup>, Hanna Axelsson<sup>1,3</sup>, Tatjana Djureinovic<sup>7,†</sup>, Jordi Carreras Puigvert<sup>1</sup>, Maria Häggblad<sup>9</sup>, Fredrik Jeppsson<sup>1</sup>, Ulf Martens<sup>9</sup>, Cecilia Lundin<sup>1</sup>, Bo Lundgren<sup>9</sup>, Ingrid Granelli<sup>5</sup>, Annika Jenmalm Jensen<sup>1,3</sup>, Per Artursson<sup>3,6</sup>, Jonas A. Nilsson<sup>4</sup>, Pål Stenmark<sup>2</sup>, Martin Scobie<sup>1</sup>, Ulrika Warpmann Berglund<sup>1</sup> & Thomas Helleday<sup>1</sup>

**Cancers have dysfunctional redox regulation resulting in reactive oxygen species production, damaging both DNA and free dNTPs. The MTH1 protein sanitizes oxidized dNTP pools to prevent incorporation of damaged bases during DNA replication. Although MTH1 is non-essential in normal cells, we show that cancer cells require MTH1 activity to avoid incorporation of oxidized dNTPs, resulting in DNA damage and cell death. We validate MTH1 as an anticancer target *in vivo* and describe small molecules TH287 and TH588 as first-in-class nudix hydrolase family inhibitors that potently and selectively engage and inhibit the MTH1 protein in cells. Protein co-crystal structures demonstrate that the inhibitors bind in the active site of MTH1. The inhibitors cause incorporation of oxidized dNTPs in cancer cells, leading to DNA damage, cytotoxicity and therapeutic responses in patient-derived mouse xenografts. This study exemplifies the non-oncogene addiction concept for anticancer treatment and validates MTH1 as being cancer phenotypic lethal.**

Anticancer treatments are dominated by targeting the genetic defects found in cancers, such as oncogenes (for example, imatinib for *BCR-ABL* mutated cancer<sup>1</sup>) or non-oncogenic genetic defects (for example, PARP inhibitors for *BRCA1* and *BRCA2* mutated cancer<sup>2,3</sup>). Although a few cases show impressive results, these treatments have, in general, not replaced radiotherapy or chemotherapy. Targeting genetic defects in a personalized strategy is limited by the high degree of intra-tumour heterogeneity, adaptation of genetic networks and high somatic mutation rates in cancer<sup>4</sup>. Here, we reasoned that a de-personalized anticancer strategy, targeting the cancer phenotype using a synthetic-lethal approach, may tackle the problem of intra-tumour heterogeneity and be more widely applicable to a range of tumours.

Altered redox regulation is a general phenotype of many cancers and has a crucial role in cancer aetiology, progression and metastasis<sup>5</sup>. Dysfunctional redox regulation and an increased reactive oxygen species (ROS) tension can cause oxidative damage to DNA directly, or to free bases in the cellular and mitochondrial deoxynucleoside triphosphate (dNTP) pool<sup>6</sup>. Damage on double-stranded DNA has been the main therapeutic focus in spite of the fact that the free dNTP precursor pool is 190–13,000 times more susceptible to damage<sup>7</sup>. The MTH1 protein sanitizes the oxidized dNTP pool, for example, by converting 8-oxodGTP or 2-OH-dATP into 8-oxodGMP or 2-OH-dAMP, thus avoiding incorporation of these oxidized nucleotides into the DNA, which otherwise

can result in mispairing, mutations and cell death<sup>8–10</sup>. Interestingly, overexpression of MTH1 suppresses the mutator phenotype in mismatch-repair-defective colorectal cancer cells<sup>11</sup>, indicating that the oxidized dNTP pool is a major source of damage causing mutations in cancer. Furthermore, overexpression of MTH1 reverses Ras-induced senescence by suppressing the overall level of DNA damage<sup>12</sup>, underscoring the importance of oxidized dNTPs in cancer. As altered redox status can be exploited for cancer treatments<sup>5</sup>, we reasoned that the normally non-essential MTH1 protein<sup>13</sup> may be important for sanitizing cancer-associated damage in the dNTP pool and required for survival in cancer cells. Here, we wanted to evaluate whether MTH1 could be a general target for cancer treatment owing to non-oncogene addiction; that is, cancer phenotypic lethal.

## MTH1 is required for cancer survival

To investigate MTH1 as a target for cancer treatment, the protein was depleted using three different short interfering RNAs (siRNAs) in several cancer cell lines, resulting in DNA damage and reduced clonogenic survival and viability; the variable degree of responses are probably due to the transient and incomplete depletion of the protein (Extended Data Fig. 1). Furthermore, rescue expression of the RNA interference (RNAi)-resistant wild-type protein, but not MTH1(E56A) catalytically dead protein, fully reversed the reduced survival in U2OS cells (Fig. 1a and Extended

<sup>1</sup>Science for Life Laboratory, Division of Translational Medicine and Chemical Biology, Department of Medical Biochemistry and Biophysics, Karolinska Institutet, S-171 21 Stockholm, Sweden.

<sup>2</sup>Department of Biochemistry and Biophysics, Stockholm University, S-106 91 Stockholm, Sweden. <sup>3</sup>Chemical Biology Consortium Sweden, Science for Life Laboratory, Division of Translational Medicine and Chemical Biology, Department of Medical Biochemistry and Biophysics, Karolinska Institutet, S-171 21 Stockholm, Sweden. <sup>4</sup>Sahlgrenska Translational Melanoma Group, Sahlgrenska Cancer Center, Department of Surgery, University of Gothenburg and Sahlgrenska University Hospital, S-405 30 Gothenburg, Sweden. <sup>5</sup>Department of Analytical Chemistry, Stockholm University, S-106 91 Stockholm, Sweden. <sup>6</sup>Uppsala University Drug Optimization and Pharmaceutical Profiling Platform, Department of Pharmacy, Uppsala University, S-751 23 Uppsala, Sweden. <sup>7</sup>Department of Genetics, Microbiology and Toxicology, Stockholm University, S-106 91 Stockholm, Sweden. <sup>8</sup>Clinical Pharmacology, Department of Medical and Health Sciences, Linköping University, S-581 85 Linköping, Sweden. <sup>9</sup>Science for Life Laboratory, RNAi Cell Screening Facility, Department of Biochemistry and Biophysics, Stockholm University, S-106 91 Stockholm, Sweden. <sup>†</sup>Present addresses: Division of Molecular Carcinogenesis, The Netherlands Cancer Institute, 1006 Amsterdam, The Netherlands (B.E.); Department of Immunology, Genetics, and Pathology, Uppsala University, S-751 23 Uppsala, Sweden (T.D.).

\*These authors contributed equally to this work.

Data Fig. 2a–c). Notably, no attenuation of survival was observed in primary VH10 cells. These cells display a lower level of carbonylated proteins, indicative of lower levels of ROS, compared to U2OS cancer cells (Extended Data Fig. 2j), in agreement with MTH1 being non-essential in normal cells and knockout mice having mild phenotypes<sup>13</sup>. MTH1 depletion in cancer cells results in the accumulation of 8-oxodG in DNA and nuclear 53BP1 foci, occurring at DNA double-strand breaks (DSBs)<sup>14</sup>. These effects are fully reversed by expression of an RNAi-resistant wild-type MTH1 but not the catalytically dead protein (Fig. 1b, c). Although 8-oxodG incorporation couldn't be confirmed by liquid chromatography-mass spectrometry (LC-MS/MS) owing to the widely reported

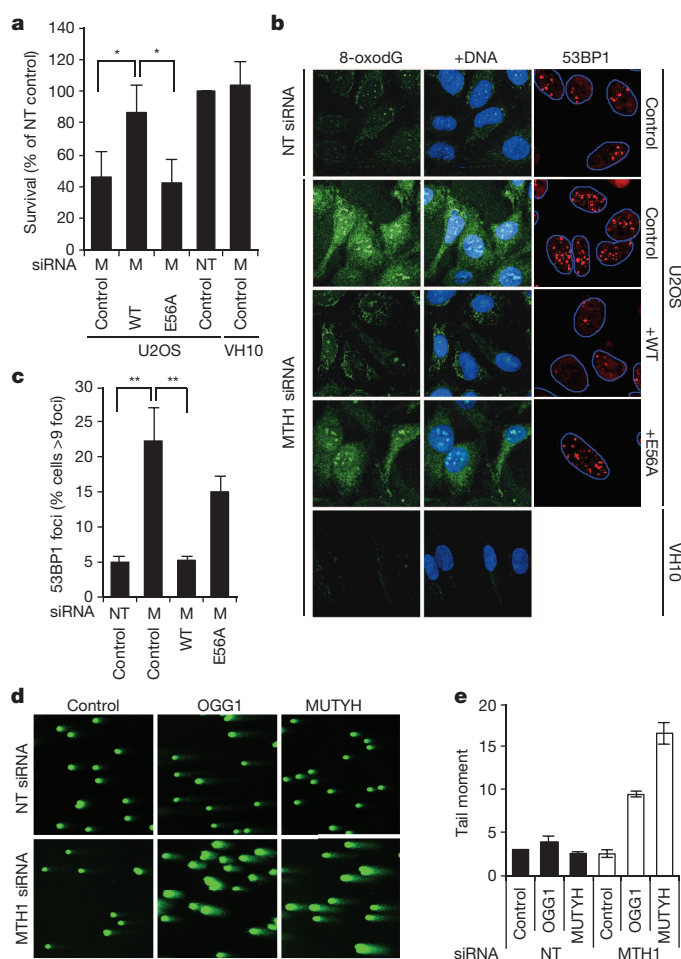


**Figure 1 | MTH1 prevents 8-oxodGTP incorporation and is required for cancer cell survival.** **a**, Clonogenic survival of U2OS and VH10 cells transiently transfected with MTH1 siRNA (M) or non-targeting siRNA (NT). Overexpression of wild-type (WT) MTH1 but not the catalytically dead mutant (E56A) reverses the decrease in survival after MTH1 knockdown. Data shown as average  $\pm$  s.d. from three independent experiments. \* $P < 0.05$ , one-way analysis of variance (ANOVA). **b**, 8-oxodG incorporation in DNA (Avidin-AlexaFluor488 reactive substance) and induction of 53BP1 foci in U2OS and VH10 cells transiently transfected with non-targeting siRNA or MTH1 siRNA for 6 days. Overexpression of wild-type MTH1 but not the catalytically dead mutant (E56A) rescues both 8-oxodG and 53BP1 foci formation. **c**, Quantification of 53BP1 foci formation in U2OS cells with overexpression of wild-type and catalytically dead mutant (E56A) after siRNA transfection for 6 days. Data shown as average  $\pm$  s.d. from three independent experiments ( $\geq 200$  cells per sample size). \*\* $P < 0.01$ , one-way ANOVA. **d**, MTH1 siRNA depletion increases 8-oxodG and 2-OH-dA levels in DNA. Alkaline comets of U2OS cells transfected with non-targeting siRNA or MTH1 siRNA no. 1, incubated with OGG1, MUTYH or buffer alone (control) for 45 min at 37 °C. **e**, Quantification of comet tail moment. Values represent average  $\pm$  s.e.m. from two independent experiments ( $> 100$  comets per experiment).

generation of oxidized bases during sample preparation<sup>15</sup>, we were able to detect 8-oxodG and 2-OH-dA in DNA by the modified Comet assay (Fig. 1d, e), using OGG1 (recognizing 8-oxodG) and MUTYH (recognizing 8-oxodG and 2-OH-dA). These data indicate that MTH1 prevents incorporation of both 8-oxodG and 2-OH-dA (ref. 16). To determine whether 8-oxodG and/or 2-OH-dA contribute to cytotoxicity after MTH1 loss, we expressed RNAi-resistant MTH1 mutants D119A and W117Y, defective in 8-oxodGTPase and 2-OH-dATPase activity, respectively<sup>16</sup>, neither of which rescued viability (Extended Data Fig. 2g–i). These data indicate that both 8-oxodG and 2-OH-dA contribute to the cytotoxicity.

DNA damage induced by MTH1 depletion activates RAD51- and DNA-PKcs-mediated DSB repair (Fig. 2), as well as ATM-dependent phosphorylation of p53 (S15) and upregulated expression of the p53 target gene *p21* (Fig. 2a, g and Extended Data Fig. 2k, l). p53 is known to mediate apoptosis after DNA damage, and short hairpin RNA (shRNA)-mediated depletion of p53 in U2OS cells prevented p21 induction and apoptosis after siRNA-mediated depletion of MTH1 (Fig. 2g–i). However, DNA damage is also induced in p53-depleted cells and the p53 status does not influence trimethylation of lysine 9 in histone H3 (H3K9me3), which is a marker for senescence<sup>17</sup> (Fig. 2h).

We next established TP53 mutant SW480 colorectal cancer cells stably carrying a doxycycline-inducible shRNA vector targeting MTH1, which when induced, reduced MTH1 expression and clonogenic survival (Fig. 2j, k). In mice, tumours with the MTH1 shRNA construct all responded when doxycycline was added to the drinking water, resulting in improved survival (Fig. 2l, m and Extended Data Fig. 2m, n). Doxycycline treatment of mice carrying tumours expressing non-targeting shRNA had no effect on tumour growth.

## Development of MTH1 inhibitors

Our data demonstrate that MTH1 catalytic activity is required for cancer cell survival, as only the RNAi-resistant wild-type MTH1, and not the catalytically dead MTH1 (E56A), restores survival. This suggests that similar effects could be obtained by MTH1 inhibition. We purified the MTH1 protein, screened compound libraries and identified small molecule hits containing a 2-aminopyrimidine motif (scaffold 1) that efficiently inhibited MTH1 catalytic activity. Introduction of an aminomethyl substituent TH086 (1) provided a marked increase in potency (Extended Data Fig. 3b–e). After hit expansion, TH287 (2) was identified as a potent MTH1 inhibitor (half-maximum inhibitory concentration (IC<sub>50</sub>) = 0.8  $\pm$  0.1 nM; Extended Data Fig. 3).

TH287 was rapidly metabolized in human and mouse liver microsomes both *in vitro* and *in vivo* via *N*-dealkylation of the aminomethyl substituent (Extended Data Table 2 and Extended Data Fig. 4a). Replacement of the methyl group by a cyclopropyl substituent in TH588 (3) improved metabolic stability both *in vitro* and *in vivo*, while maintaining MTH1 potency (IC<sub>50</sub> = 5.0  $\pm$  0.2 nM) (Extended Data Figs 3 and 4b, c and Extended Data Table 2). In contrast, introduction of an oxetanyl ring in TH650 (4) also improved metabolic stability but markedly reduced MTH1 potency (IC<sub>50</sub> = 2.1  $\pm$  0.1  $\mu$ M). Using a target engagement assay<sup>18</sup> we observed that MTH1 inhibitors TH287 and TH588, but not TH650, bind the MTH1 protein in cells.

## MTH1 inhibitor co-crystals

To gain further insight into the mechanism of how TH287 and TH588 inhibit MTH1, we determined the structures of MTH1 in complex with TH287 and TH588 to a resolution of 1.6 Å (Fig. 3, Extended Data Table 1 and Extended Data Fig. 3i, j). The aminopyrimidine moiety in TH287 and TH588 binds in the active site with key hydrogen bonds to Asn 33, Asp 119 and Asp 120 (Fig. 3b–d). As a result of the cyclopropyl substitution in TH588 the dichlorophenyl ring has rotated approximately 180° between TH287 and TH588. The aminomethyl substituent in TH287 and the corresponding amino group in TH588 appear to be a feature that is important for affinity and specificity, and we speculate that the

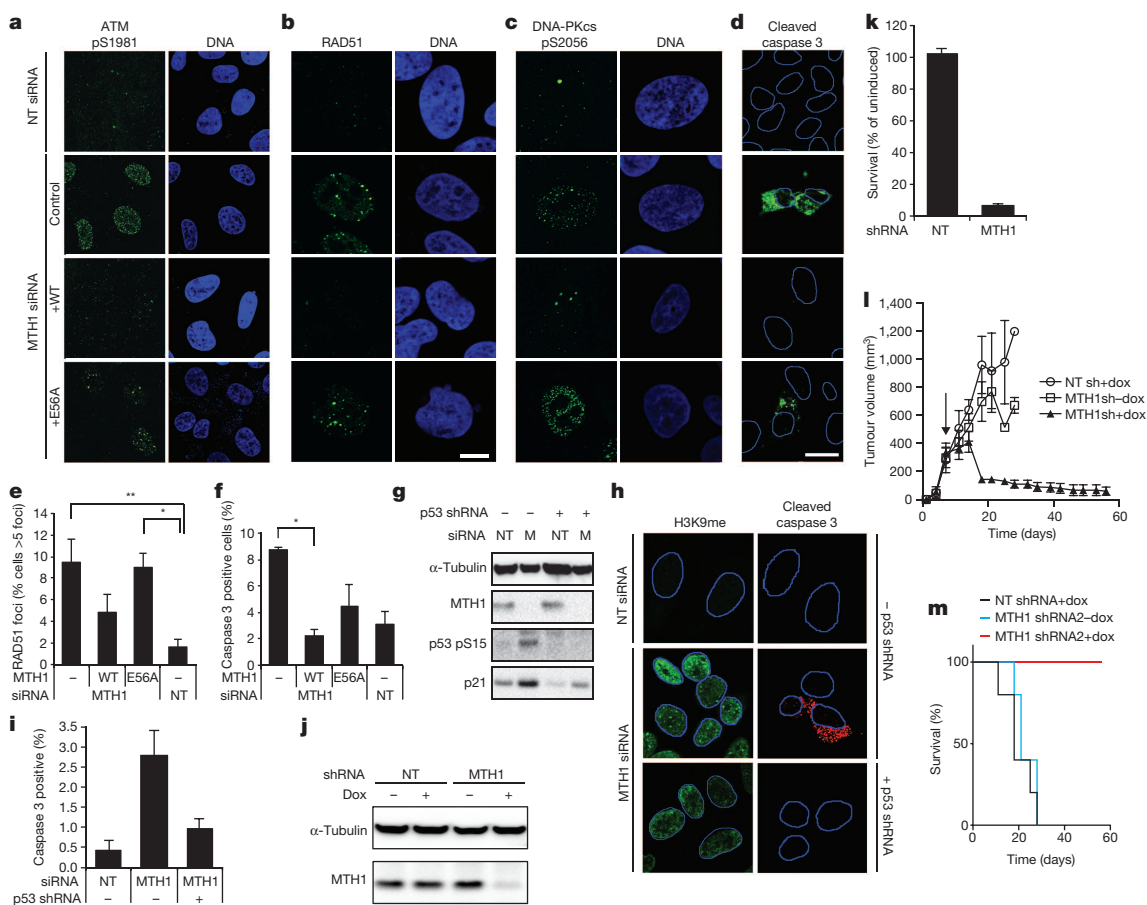


**Figure 2 | MTH1 activity is required to prevent DNA damage and promote tumour growth in xenograft mice.** **a–d**, After *MTH1* siRNA treatment, ATM autophosphorylation at serine 1981 (**a**), RAD51 foci (**b**), phosphorylated DNA-PKcs pS2056 foci (**c**) and caspase 3 cleavage (apoptosis) (**d**) were visualized. Expression of siRNA-resistant *MTH1* wild-type prevents ATM activation, RAD51 foci, DNA-PKcs pS2056 foci and apoptosis but not expression of *MTH1* catalytically dead mutant (E56A). Nuclei are indicated with thin blue lines. Scale bar, 10  $\mu\text{m}$ . **e**, Quantification of RAD51 foci. Data shown as average  $\pm$  s.e.m. from three independent experiments ( $\geq 200$  cells per sample). \* $P < 0.05$ , \*\* $P < 0.01$ , one-way ANOVA. **f**, Quantification of cleaved-caspase-3-positive cells from panel **d**. Data shown as average  $\pm$  s.e.m. from two independent experiments ( $P < 0.05$ , one-way ANOVA). **g, h**, Western blot (**g**) and immunofluorescence (**h**) of U2OS cells depleted of p53 by doxycycline-inducible shRNA expression (p53 shRNA) and transfected with non-targeting siRNA (NT) or *MTH1* siRNA (M). **h**, Images of cells immunostained for

apoptosis (cleaved caspase 3) and senescence (H3K9me3). Nuclei are indicated with thin blue lines. **i**, Quantification of cleaved caspase 3 cells from panel **d**. Data shown as average  $\pm$  s.d. from two independent experiments. **j**, Western blot of protein lysates isolated from SW480 cells with either non-targeting shRNA or *MTH1* shRNA after 72-h treatments with  $2 \mu\text{g ml}^{-1}$  doxycycline (dox) in the medium. **k**, Clonogenic survival of SW480 cells of the cells in panel **j**. Cells were treated with doxycycline for 72 h and re-seeded for colony outgrowth. Values are indicated as survival compared to non-doxycycline-treated control cells and represent average  $\pm$  s.d. from three independent experiments. **l, m**, SW480 cells expressing doxycycline-inducible *MTH1* shRNA or non-targeting shRNA were injected into SCID mice (subcutaneous) ( $n = 5$  per group). After 7 days, doxycycline was added (arrow) to the drinking water. **l, m**, Tumour volume decreased (**l**) and survival increased in xenograft mice (**m**) with *MTH1* shRNA depletion.

hydrogen bond between NH and Asp 119 could mimic the 6-enol state of 8-oxodGTP suggested previously to be important for specificity<sup>16,19</sup>.

### MTH1 inhibitors cause cancer cell death

We observed that the *MTH1* inhibitors TH287 and TH588 selectively and effectively kill U2OS and other cancer cell lines, but were considerably less toxic to several primary or immortalized cells (Fig. 4c and Extended Data Fig. 5j–m). This is in agreement with *MTH1* being required for cancer cell survival while being non-essential in untransformed cells. The structurally similar compound TH650, which does not engage or inhibit the *MTH1* protein in cells, is not toxic in any cells tested, supporting inhibition of *MTH1* as a mechanism of induced cytotoxicity for TH287 and TH588 (Extended Data Fig. 5n). Notably, although the *MTH1* inhibitors are low-nanomolar enzymatic inhibitors they are only cytotoxic at low micromolar concentrations. This is not an uncommon phenomenon and may be explained by pharmacokinetic and/or pharmacological properties such as high protein binding or low permeability/efflux in cancer cells (Extended Data Table 2).

Compounds that exert their toxicity through *MTH1* inhibition would be expected to increase 8-oxodG incorporation into DNA. Indeed, we observed an increase of 8-oxodG in DNA after TH287 and TH588 treatment in U2OS cells, but not in VH10 cells or after treatment with TH650 (Fig. 4d–g and Extended Data Fig. 5a, c), in line with our proposed mechanism of action. Also, *MTH1* inhibitors TH287 and TH588 both induce DNA damage (53BP1, RPA and phospho-DNA-PKcs foci) and trigger an ATM-p53-mediated death response and DNA repair in U2OS cells, but not in VH10 cells (Fig. 4h and Extended Data Fig. 6). However, p53 status does not influence survival on treatment with either TH287 or TH588 (Extended Data Fig. 5f–i), which is explained by DNA damage being introduced independently of p53 status. Overall, the *MTH1* inhibitors induced a similar DNA damage response and cell death mechanism as observed after *MTH1* siRNA depletion. Although the OGG1 and MUTYH proteins are important in repair of 8-oxodG and 2-OH-dA lesions in DNA<sup>20</sup>, differential expression levels or over-expression of either OGG1 or MUTYH did not alter the cytotoxic effect of *MTH1* inhibitors (Extended Data Figs 7 and 8f), which is potentially

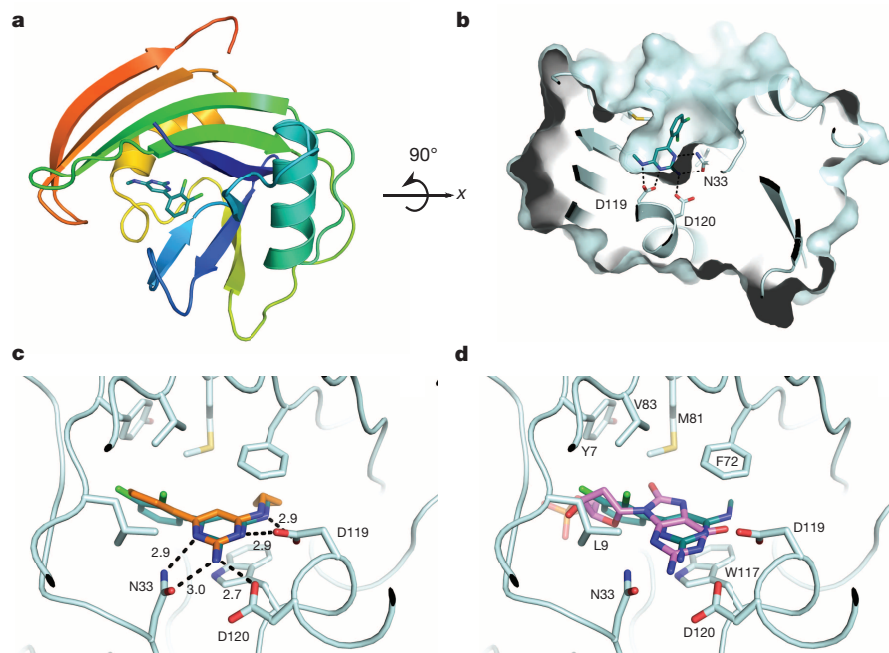


**Figure 3 | Structural details of TH287 binding to MTH1.** **a**, Overall structure of MTH1 shown in cartoon representation and coloured blue to red from amino to carboxy terminus. The bound TH287 inhibitor is shown in sticks representation. **b**, Sliced surface representation, highlighting the deep pocket of MTH1 (cyan) where TH287 (dark teal) is bound. The three residues that form

hydrogen bonds to TH287 are marked in the figure. **c**, Close-up view of the binding site, comparing the TH287 (dark teal) ligand with the TH588 (orange) ligand, with the hydrogen bonding distance marked out in Å. **d**, Comparison of TH287 (dark teal) and 8-oxodGMP (violet) binding to MTH1, with important residues in the binding site marked.

explained by an overload of oxidized bases in DNA, overwhelming the base excision repair system, or that 8-oxodGTP or 2-OH-dATP may potentially signal for cell death<sup>21</sup>. Also, the expression levels of OGG1, MUTYH or MTH2 were unaltered after MTH1 depletion (Extended Data Figs 8b–d).

To determine at which point in the cancer transformation process cells become sensitive to MTH1 inhibitors, a genetic system was used where primary BJ cells are transformed in a step-wise transfection protocol using hTERT, SV40 large T antigen and Ras<sup>22</sup>. TH287 and TH588 were selectively cytotoxic to SV40-large-T- and Ras-expressing BJ cells (Fig. 4i and Extended Data Fig. 5o, q), demonstrating that MTH1 becomes important early on in the transformation process, when MTH1 expression also increases (Extended Data Fig. 7).

### MutT rescues MTH1 inhibitor toxicity

Many small molecules are known to be promiscuous, for example several kinase inhibitors bind to multiple kinase targets. Because TH287 and TH588 are first-in-class inhibitors of the nudix hydrolase protein family, we wanted to determine how selective these compounds would be towards other members of the nudix protein family<sup>23</sup>. MTH2, NUDT5, NUDT12, NUDT14, NUDT16 and other proteins with known nucleoside triphosphate pyrophosphatase activity, that is, dCTPase, dUTPase and ITPA, were therefore expressed, purified and used to develop enzymatic activity assays. TH287 and TH588 were highly selective towards MTH1, with no relevant inhibition of any of the other tested proteins at 100  $\mu\text{M}$  (Fig. 5a and Extended Data Fig. 8h, i). Although TH588 showed reasonable selectivity when tested on a much larger panel of 87 enzymes, GPCRs, kinases, ion channels and transporters at 10  $\mu\text{M}$  (Extended Data Fig. 8g), it may still have other relevant off-target activities which are not yet known. In an effort to address this possibility, we purified the *Escherichia coli* MutT protein, which is the bacterial homologue of MTH1 (ref. 24) and has 8-oxodGTPase activity. We demonstrate that MutT is not inhibited by either TH287 or TH588 (Fig. 5b). Notably, MutT enzyme expressed in mitochondria or the nucleus (Extended Data Fig. 8k–m) partly rescues the cells from cytotoxicity and 53BP1 induction caused by TH287 and TH588 (Fig. 5c, d), demonstrating that restoration of

8-oxodGTPase activity in human cells reduces the toxicity of the compounds. The reason why MutT does not completely reverse compound toxicity is probably explained by its lack of 2-OH-dATPase activity<sup>25</sup>, which is also contributing to toxicity.

### In vivo activity of MTH1 inhibitors

Our data suggest that MTH1 inhibition may be a useful strategy to target cancer. Malignant melanomas are heterogeneous, exhibit high numbers of somatic mutations<sup>4</sup> and are generally resistant to treatments. Metastases derived from a patient with *BRAF*<sup>V600E</sup>-mutated melanoma, resistant to carboplatin, dacarbazine and vemurafenib, was serially transplanted twice in mice. Ten mice carrying this tumour were randomized to receive TH588 once daily or vehicle control treatment. All TH588-treated mice responded with a reduced tumour growth rate, even though pharmacokinetic studies had shown that the serum level of TH588 dropped below IC<sub>50</sub> concentrations during the 24-h treatment (Fig. 5e, f). In addition, SW480 colorectal and MCF7 breast tumour xenografts also responded to once-daily TH588 treatment (Extended Data Fig. 4), supporting the view that targeting MTH1 is potentially useful for a range of different tumours.

### Discussion

Here, we observe that the MTH1 protein is required for efficient survival of cancer cells, whereas it is non-essential in untransformed cells. To explain this phenomenon, we propose a model where dysfunctional redox regulation and ROS in cancer cells lead to an oxidized dNTP pool, which in turn requires the MTH1 protein to prevent incorporation and DNA damage after replication (Fig. 5g). MTH1 is found to be overexpressed in many cancers<sup>26</sup> (Extended Data Fig. 7) and the MTH1 catalytic activity is also markedly increased in lung cancer tissue<sup>26</sup>, which is an example of non-oncogene addiction and probably a survival response to prevent incorporation of oxidized dNTPs. Possible reasons why normal cells seem to be less dependent on MTH1 activity could be due to rigid redox regulation in normal cells as compared to cancer cells, and/or intact cell cycle checkpoints responding to ROS<sup>27</sup> (Fig. 5g). Our rather simple model can potentially be complicated by the fact that

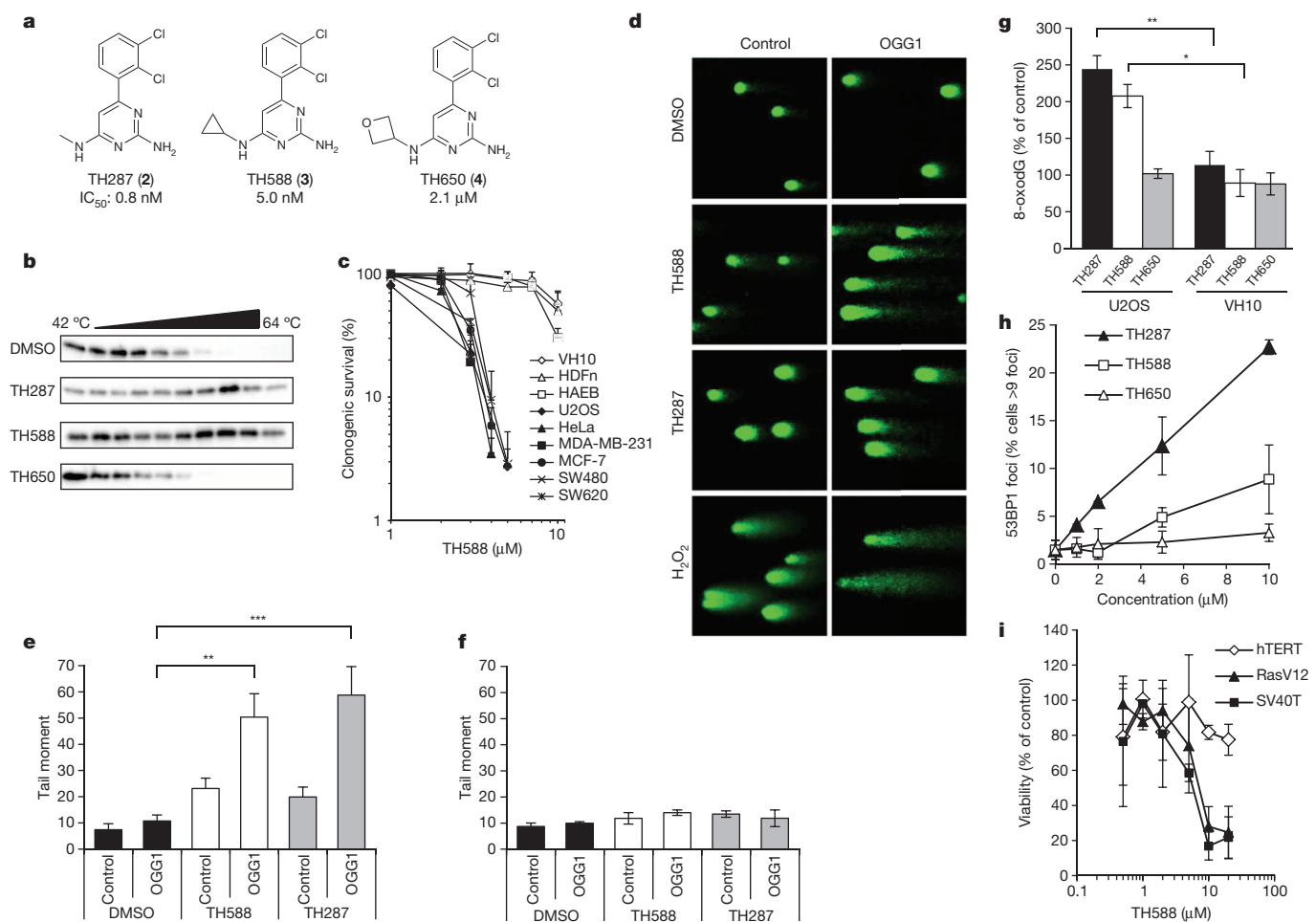


**Figure 4 | Inhibition of MTH1 induces oxidative DNA damage and reduces survival in cancer cells.** **a**, Chemical structure of the MTH1 inhibitors TH287 and TH588 and the poor inhibitor TH650. IC<sub>50</sub> values shown as average of three independent experiments. **b**, Target engagement of MTH1 inhibitor to MTH1 protein in intact cells. The MTH1 protein precipitates in cells above 54 °C. Potent MTH1 inhibitors stabilize the MTH1 protein >54 °C. **c**, Clonogenic survival of primary/immortalized (open) or cancer cells (filled) after TH588 treatment. Values represent percentage of colonies in relation to DMSO-treated controls displayed as average  $\pm$  s.d. from three independent experiments. **d–f**, U2OS cells (**d**, **e**) or VH10 cells (**f**) were treated with 10  $\mu$ M MTH1 inhibitor for 24 h before being incubated with OGG1, to selectively cut out 8-oxodG from DNA, and run in alkaline Comet assay. H<sub>2</sub>O<sub>2</sub> was used as control. Tail moment, calculated as % DNA in the tail multiplied by the tail

length. Values represent average  $\pm$  s.e.m. from three experiments; \*\* $P < 0.01$ , \*\*\* $P < 0.001$ , one-way ANOVA. **g**, Quantification of 8-oxodGTP incorporation in DNA (avidin-AlexaFluor488 reactive substance) in U2OS and VH10 cells treated with MTH1 inhibitors (20  $\mu$ M). Bars show average  $\pm$  s.e.m. of three independent experiments. Asterisks mark a significant difference (\* $P < 0.05$ , \*\* $P < 0.01$ , one-sided Student's *t*-test). **h**, U2OS cells were seeded in 96-well plates and treated with MTH1 inhibitors for 72 h and 53BP1 foci formation determined. Values represent percentage of cells with >9 53BP1 foci per cell, average  $\pm$  s.e.m. from three experiments. **i**, Viability of BJ cells with hTERT, hTERT/SV40T ('SV40T') or hTERT/SV40T/RasV12 ('RasV12') after 72 h TH588 treatment. Data shown as average  $\pm$  s.e.m. from two independent experiments.

cancer cells may adapt to imbalanced redox status and activate powerful antioxidant mechanisms to allow survival, and therefore lower the overall ROS levels in cancer. Hence, re-balancing or further alterations of the redox status may hypothetically be a resistance mechanism to MTH1 inhibitors.

Previously, overexpressed MTH1 has been demonstrated to prevent Ras-induced DNA damage<sup>12</sup>, and compounds selectively killing Ras-expressing cells are found, in a concurrent report, to work through targeting MTH1<sup>28</sup>. Here, we observe a similar cellular sensitivity to MTH1 inhibitors or siRNA in SV40 large T transfected BJ cells as those additionally transformed by Ras (Fig. 4i and Extended Data Figs 1 and 5), indicating that Ras expression is not a major determinant for the essential role of MTH1 in cancer.

MTH1 overexpression in mice promotes longevity<sup>29</sup>, reduced anxiety<sup>29</sup> and protects from 3-nitropropionic-acid-induced neurodegeneration<sup>30</sup>. Upon pathological examination of ageing *Mth1*<sup>-/-</sup> mice a slight increase in cancer incidence is observed when grouping incidences in lung, liver and stomach cancers<sup>13</sup>, whereas *Mth1* gene disruption concomitantly

suppresses lung cancer development in *Ogg1*<sup>-/-</sup> mice<sup>31</sup>. These data suggest that long-term MTH1 inhibitor treatments may be associated with non-acute side effects, similar to those observed with PARP inhibitors. However, MTH1 inhibition may still be an interesting approach considering many anticancer target proteins are essential and severe side effects are associated with current chemotherapies.

Here we present first-in-class inhibitors to the nudix hydrolase protein family, which show excellent selectivity against other nudix family proteins and good selectivity towards kinases present in the selectivity panel. We expressed the bacterial MutT protein to rescue 8-oxodGTPase activity in cells in the presence of MTH1 inhibitors. We observed that MutT expression partly restores cellular viability and decreases DSB formation (53BP1 foci; Fig. 5). Proving that restoration of biochemical activity can rescue a biological effect is the ultimate proof for on-target effects of compounds and we suggest that such experiments should be used more widely.

In conclusion, we demonstrate that targeting MTH1 constitutes a novel cancer phenotypic lethal anticancer therapeutic approach targeting

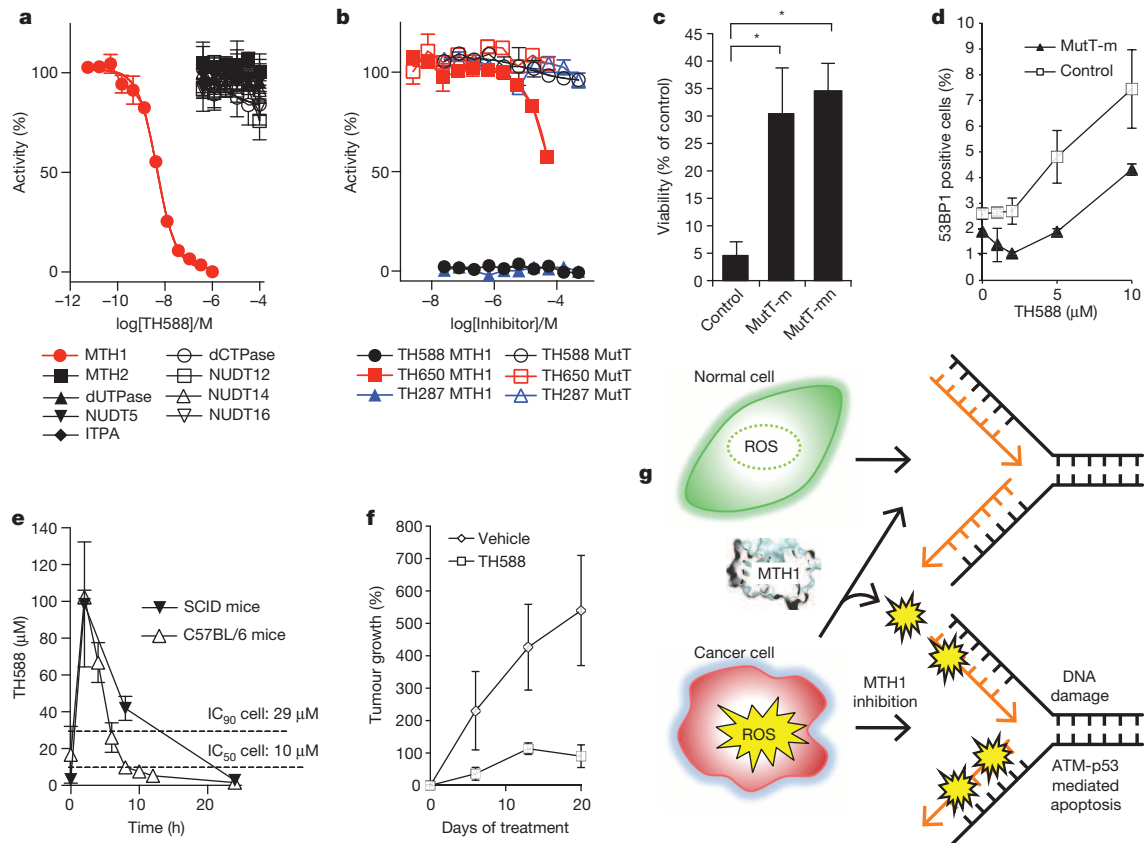


**Figure 5 | TH588 reduces tumour growth via MTH1 inhibition.** **a**, *In vitro* activity of human MTH1, MTH2 (NUDT15), NUDT5, NUDT12, NUDT14, NUDT16, dUTPase, dCTPase and ITPA treated with varying concentrations of the MTH1 inhibitor TH588. Data shown as average  $\pm$  s.d. of three to six individual experiments, each performed in duplicate. **b**, MTH1 inhibitors TH287, TH588 and TH650 do not inhibit MutT. Inhibitory potency of TH287, TH588 and TH650 was tested against MutT (9.6 nM) and MTH1 (4.75 nM) at 100  $\mu$ M dGTP and various inhibitor concentrations. Data shown as average  $\pm$  s.d. from two independent experiments. **c**, **d**, Viability (**c**) and 53BP1 foci formation (**d**) in U2OS cells overexpressing MutT localized to the mitochondria (MutT-m) or MutT localized to both the mitochondria and nucleus (MutT-mn) or with no overexpression (control) treated with 10  $\mu$ M

TH588 for 72 h. Data shown as average  $\pm$  s.d., \*\* $P < 0.01$ , one-way ANOVA. Values represent average  $\pm$  s.e.m. from three independent experiments. **e**, Plasma exposure of TH588 after 3 days treatment in C57BL/6 ( $n = 3$  per time point) and SCID mice ( $n = 3$  per time point) with subcutaneous injections of 25 mg kg<sup>-1</sup> TH588; plasma exposure was measured after the third injection on day 3. The dotted lines indicate the IC<sub>50</sub> and IC<sub>90</sub> values obtained from cell survival *in vitro* in SW480 cells. **f**, Growth of visceral metastasis from a malignant melanoma patient in NOD-scid IL2R $\gamma$ <sup>null</sup> (NOG) mice treated once daily with TH588 (30 mg kg<sup>-1</sup>, subcutaneous administration, once daily) or vehicle ( $n = 5$  per group). **g**, Model for MTH1-dependent survival in cancer cells.

non-oncogene addiction, which converts deregulated metabolism and ROS levels present in cancer into toxic DNA damage.

## METHODS SUMMARY

Cells were cultivated in suitable medium supplemented with 10% FBS at 37 °C at 5% CO<sub>2</sub>. MTH1-puro vector was a gift from R. Weinberg. The siRNA-resistant MTH1 vector was made by site-directed mutagenesis of codons GAC and AGC at position 384–389 into GAT and TCC, coding for the same amino acids. The E56A mutant was generated by site-directed mutagenesis.

**Online Content** Any additional Methods, Extended Data display items and Source Data are available in the online version of the paper; references unique to these sections appear only in the online paper.

Received 22 March 2013; accepted 20 February 2014.

Published online 2 April 2014.

1. Druker, B. J. *et al.* Effects of a selective inhibitor of the Abl tyrosine kinase on the growth of Bcr-Abl positive cells. *Nature Med.* **2**, 561–566 (1996).
2. Bryant, H. E. *et al.* Specific killing of BRCA2-deficient tumours with inhibitors of poly(ADP-ribose)polymerase. *Nature* **434**, 913–917 (2005).
3. Farmer, H. *et al.* Targeting the DNA repair defect in BRCA mutant cells as a therapeutic strategy. *Nature* **434**, 917–921 (2005).
4. Alexandrov, L. B. *et al.* Signatures of mutational processes in human cancer. *Nature* **500**, 415–421 (2013).
5. Zhang, Y. *et al.* Redox control of the survival of healthy and diseased cells. *Antioxid. Redox Signal.* **15**, 2867–2908 (2011).

6. Luo, M., He, H., Kelley, M. R. & Georgiadis, M. M. Redox regulation of DNA repair: implications for human health and cancer therapeutic development. *Antioxid. Redox Signal.* **12**, 1247–1269 (2010).
7. Topal, M. D. & Baker, M. S. DNA precursor pool: a significant target for N-methyl-N-nitrosourea in C3H/10T1/2 clone 8 cells. *Proc. Natl Acad. Sci. USA* **79**, 2211–2215 (1982).
8. Sakumi, K. *et al.* Cloning and expression of cDNA for a human enzyme that hydrolyzes 8-oxo-dGTP, a mutagenic substrate for DNA synthesis. *J. Biol. Chem.* **268**, 23524–23530 (1993).
9. Oka, S. *et al.* Two distinct pathways of cell death triggered by oxidative damage to nuclear and mitochondrial DNAs. *EMBO J.* **27**, 421–432 (2008).
10. Ichikawa, J. *et al.* Oxidation of mitochondrial deoxynucleotide pools by exposure to sodium nitroprusside induces cell death. *DNA Repair (Amst.)* **7**, 418–430 (2008).
11. Russo, M. T. *et al.* The oxidized deoxynucleoside triphosphate pool is a significant contributor to genetic instability in mismatch repair-deficient cells. *Mol. Cell. Biol.* **24**, 465–474 (2004).
12. Rai, P. *et al.* Enhanced elimination of oxidized guanine nucleotides inhibits oncogenic RAS-induced DNA damage and premature senescence. *Oncogene* **30**, 1489–1496 (2011).
13. Tsuzuki, T., Egashira, A. & Kura, S. Analysis of MTH1 gene function in mice with targeted mutagenesis. *Mutat. Res.* **477**, 71–78 (2001).
14. Schultz, L. B., Chehab, N. H., Malikzay, A. & Halazonetis, T. D. p53 binding protein 1 (53BP1) is an early participant in the cellular response to DNA double-strand breaks. *J. Cell Biol.* **151**, 1381–1390 (2000).
15. European Standards Committee on Oxidative DNA Damage. Measurement of DNA oxidation in human cells by chromatographic and enzymic methods. *Free Radic. Biol. Med.* **34**, 1089–1099 (2003).
16. Yoshimura, D. *et al.* An oxidized purine nucleoside triphosphatase, MTH1, suppresses cell death caused by oxidative stress. *J. Biol. Chem.* **278**, 37965–37973 (2003).

17. Narita, M. *et al.* Rb-mediated heterochromatin formation and silencing of E2F target genes during cellular senescence. *Cell* **113**, 703–716 (2003).
18. Martinez Molina, D. *et al.* Monitoring drug target engagement in cells and tissues using the cellular thermal shift assay. *Science* **341**, 84–87 (2013).
19. Svensson, L. M. *et al.* Crystal structure of human MTH1 and the 8-oxo-dGMP product complex. *FEBS Lett* **585**, 2617–2621 (2011).
20. Ushijima, Y. *et al.* A functional analysis of the DNA glycosylase activity of mouse MUTYH protein excising 2-hydroxyadenine opposite guanine in DNA. *Nucleic Acids Res.* **33**, 672–682 (2005).
21. German, P. *et al.* Activation of cellular signaling by 8-oxoguanine DNA glycosylase-1-initiated DNA base excision repair. *DNA Repair (Amst.)* **12**, 856–863 (2013).
22. Hahn, W. C. *et al.* Creation of human tumour cells with defined genetic elements. *Nature* **400**, 464–468 (1999).
23. McLennan, A. G. Substrate ambiguity among the nudix hydrolases: biologically significant, evolutionary remnant, or both? *Cell. Mol. Life Sci.* **70**, 373–385 (2013).
24. Maki, H. & Sekiguchi, M. MutT protein specifically hydrolyses a potent mutagenic substrate for DNA synthesis. *Nature* **355**, 273–275 (1992).
25. Fujikawa, K. *et al.* The oxidized forms of dATP are substrates for the human MutT homologue, the hMTH1 protein. *J. Biol. Chem.* **274**, 18201–18205 (1999).
26. Speina, E. *et al.* Contribution of hMTH1 to the maintenance of 8-oxoguanine levels in lung DNA of non-small-cell lung cancer patients. *J. Natl Cancer Inst.* **97**, 384–395 (2005).
27. Guo, Z., Kozlov, S., Lavin, M. F., Person, M. D. & Paull, T. T. ATM activation by oxidative stress. *Science* **330**, 517–521 (2010).
28. Huber, K. V. M. *et al.* Stereospecific targeting of MTH1 by (S)-crizotinib as an anticancer strategy. *Nature* <http://dx.doi.org/10.1038/nature13194> (this issue).
29. De Luca, G. *et al.* Prolonged lifespan with enhanced exploratory behavior in mice overexpressing the oxidized nucleoside triphosphatase hMTH1. *Aging Cell* **12**, 695–705 (2013).
30. De Luca, G. *et al.* A role for oxidized DNA precursors in Huntington's disease-like striatal neurodegeneration. *PLoS Genet.* **4**, e1000266 (2008).
31. Sakumi, K. *et al.* *Ogg1* knockout-associated lung tumorigenesis and its suppression by *Mth1* gene disruption. *Cancer Res.* **63**, 902–905 (2003).

**Supplementary Information** is available in the online version of the paper.

**Acknowledgements** We thank scientists at BESSY, ESRF, Max-Lab and the Swiss Light Source for structural biology data collection support, PSF for protein purification, GE Healthcare for instrument access, HTSRC (Rockefeller University) for iTC<sub>200</sub> calorimeter access, S. Nordstrand for animal support, and L. Ny, U. Stierner and J. Mattsson for discussions. The Helleday Laboratory is primarily funded by the Torsten and Ragnar Söderberg Foundation (T.H.). This project is primarily supported by The Knut and Alice Wallenberg Foundation. Further support was received from the Swedish Research Council (T.H., A.J.J., P.A., P.S., J.A.N.), the European Research Council (T.H.), Swedish Cancer Society (T.H., J.A.N.), the Swedish Children's Cancer Foundation (T.H.), AFA insurance (T.H.), the Swedish Pain Relief Foundation (T.H.), The Cancer Society in Stockholm (T.H.), the Wenner-Gren Foundations (P.S.), the Swedish Foundation for Strategic Research (P.S.), the Dutch Cancer Society (B.E.), EMBO LTF (R.B.), Region Västra Götaland (J.A.N.), BioCARE (J.A.N.), the Swiss National Science Foundation (F.Z.G.) and the Nicholson Exchange Program (T.L.). Chemical Biology Consortium Sweden (CBCS) is primarily funded by the Swedish Research Council. CBCS acknowledge Swedish Orphan Biovitrum for their donation of a small-molecule infrastructure including a compound collection.

**Author Contributions** T.H. devised concept and supervised the project. H.G., S.E., N.S., C.E.S., L.B., K.Sa., F.Jo., A.Hö., B.E., T.D., M.A., A.Ha., C.L., U.W.B. and T.H. designed, performed and analysed cell biology experiments. A-S.J., T.L., F.Je., O.L., K.St., T.K., M.Hä., U.M., B.L., L.J., A.J.J., E.W., C.K., I.A., S.A.J., U.W.B. and T.H. designed, performed and analysed biochemical and high-throughput experiments. L.M.S., R.P.-A.B., R.G. and P.S. designed, performed and analysed structural biology experiments. T.K., S.A.J., M.D., M.-C.J.-C., L.J., L.G.J.H., M.He, K.S.A.V., O.A.W., A.J.J., M.S. and T.H. designed, performed and analysed medicinal chemistry experiments. A.-L.G., J.C.P., E.J.H. and M.D. performed computational chemistry analysis and/or support. C.G., B.O.E., A.S., K.Sa., P.B., R.S., F.Z.G., I.G., P.A., T.P., S.V., J.A.N. and U.W.B. designed, performed and analysed ADME, pharmacology and *in vivo* experiments. R.O. performed surgery, and clinical follow-up. H.G., U.W.B. and T.H. wrote the paper. All authors discussed results and approved the manuscript.

**Author Information** Reprints and permissions information is available at [www.nature.com/reprints](http://www.nature.com/reprints). Readers are welcome to comment on the online version of the paper. The authors declare competing financial interests: details are available in the online version of the paper. Correspondence and requests for materials should be addressed to T.H. ([thomas.helleday@scilifelab.se](mailto:thomas.helleday@scilifelab.se)).

## METHODS

**Antibodies.** The following antibodies were used: rabbit anti-53BP1 (A300-272A, Bethyl Laboratories), rabbit anti-Rad51 (H92, Santa Cruz Biotech), mouse anti-Rad51 (14B4, Abcam), rat anti-RPA32 (E4A, Cell Signaling Technologies), mouse anti-ATM pS1981 (sc47739, Santa Cruz Biotech), rabbit anti-p53 pS15 (Cell Signaling Technologies), mouse anti-p53 (DO-1, Santa Cruz Biotech), rabbit anti-DNA-PKcs pS2056 (Abcam), rabbit anti-MTH1 (gift from HPA, Royal School of Technology), rabbit anti-MTH1 (Novus Biologicals), rabbit anti-cleaved caspase 3 (Cell Signaling Technologies), rabbit anti-histone H3me3 K9 (Millipore), mouse anti-c-Myc (9E10, Santa Cruz Biotech), mouse anti- $\alpha$ -tubulin (Sigma Aldrich), rabbit anti-p21 (H164, Santa Cruz Biotech), mouse anti- $\beta$ -actin (Sigma Aldrich). **Cell culture.** Cells were cultivated in suitable medium supplemented with 10% FBS and 10 U ml<sup>-1</sup> penicillin/streptomycin (PeSt, Invitrogen) at 37 °C at 5% CO<sub>2</sub>. U2OS, SW480.SN3, SW620, HCT116, HeLa, HEK-293T, HepG2, MB231 and HEC59 cells were cultivated in DMEM; LNCaP, DU145, HCC38, VACO4B, Cco-7, T47D and HCC1937 were grown in RPMI-1640 (ATCC); PC-3 were cultivated in F-12; Glioma A were grown in MEM; BJ-hTERT, BJ-SV40T, BJ-RasV12, MRC-9 and VH10 were cultivated in DMEM high glucose. The BJ-hTERT, BJ-SV40T and BJ-RasV12 were provided by W. Hahn (Dana-Farber Cancer Institute). U2OS, HEK-293T, HCC1937, MB231, HCT-116, HCC38, HeLa, MCF-7, PC-3, T47D, LNCaP and HepG2 were from ATCC, DU-145 from DSMZ. SW480.SN3 originated from SW480 cells<sup>32</sup>, SW620, HEC59, VACO4B and Cco-7 from Walter Bodmer (Oxford University), and Glioma A from M. Nistér (Karolinska Institutet). All melanoma cell lines used in the study were purchased from Cell line Services and were cultured in media specified by the provider. All cell lines were used within three passages after purchase.

**RNA preparation and analysis.** RNA from cultured cells was isolated using Trizol reagent (Invitrogen) and the Direct-zol RNA miniprep kit (Zymo Research). cDNA synthesis was performed on 500 ng RNA using the iScript cDNA synthesis kit (BioRad). qRT-PCR was performed using the iTaq Universal SYBR Green Supermix (BioRad), cDNA and primers directed against MTH1 (GenBank accession number D38594.2), MTH2 (GenBank accession number BC133017.1), NUDT5 (GenBank accession number BC000025.2), MUTYH (GenBank accession number AF527839.1), OGG1 (GenBank accession number AB000410.1), GAPDH and  $\beta$ -actin on a CFX96 real-time PCR machine (BioRad). Relative mRNA levels were calculated using the BioRad software, comparing expression of the genes using primers hGAPDH\_F: 5'-AAGTTCGGAGTCAACGGATT-3', hGAPDH\_R: 5'-CTCCTGGAAGATGGTATGG-3',  $\beta$ -actin\_F: 5'-CCTGGCACCCAGCACAA T-3',  $\beta$ -actin\_R: 5'-GGGCCGGACTCGTCATAC-3', 18s rRNA\_F: 5'-AGTCC CTGCCCTTTGTACACA-3', 18s rRNA\_R: 5'-GATCCGAGGGCCCTCACTAAA C-3', MTH1\_F: 5'-GTGCAGAACCCAGGGACCAT-3', MTH1\_R: 5'-GCCAC GAACCTCAAAACGCA-3', MTH2\_F: 5'-TGTTCACTTTGCCTCAGTTGTG-3', MTH2\_R: 5'-AGGAACCCACTCCCACTTC-3', NUDT5\_F: 5'-TCCTTTTA GCACCGGAGAG-3', NUDT5\_R: 5'-CAGGTGAGAAAGTTCCACTCCAA-3', MUTYH\_F: 5'-TTCTGCCTGTGATGGCCTG-3', MUTYH\_R: 5'-GTCCCGTT TCTCTGGTTCGT-3', OGG1\_F: 5'-ACAATCTTCCGGTGGAGGG-3', OGG 1\_R: 5'-TGGCTCTTGTCTCCTCGGTA-3'.

**Eukaryotic expression constructs.** The MTH1-puro vector was a gift from R. Weinberg<sup>33</sup>. The siRNA-resistant MTH1 vector was made by site-directed mutagenesis of codons GAC and AGC at position 384–389 into GAT and TCC, coding for the same amino acids. The E56A mutant was generated by site-directed mutagenesis using the primer 5'-GGGAGCTGCAGGAGGCAAGCGGTCTGACAGT GGAC-3' and the reverse complement primer. siRNA-resistant cDNA encoding MTH1(W117Y) and MTH1(D119A) mutants were generated by site-directed mutagenesis using the primers 5'-CCCTCAAGGACATGTACCCGACGATTCTCT AC-3' (W117Y) and 5'-GGACATGTGGCCCGGATTCCTACTGGTTTC-3' (D119A) and their reverse complement primers and siRNA-resistant pBabepuro MTH1 as template followed by subcloning into pBabepuro using BamHI and EcoRI. The mutations were verified by sequencing. *Escherichia coli* MutT was cloned from genomic *E. coli* DNA. The MutT-nuc vector was generated by PCR amplification of MutT cDNA using the primers 5'-TATAGGATCCACCATGAAAAAGC TGCAAATTCGGGTAGG-3' and 5'-TATACTCGAGCAGACGTTAAGCTT CGCAATTAC-3' with BamHI and XhoI restriction sites, respectively. After restriction digest, MutT was ligated into pcDNA3.1mycHisA-vector (Invitrogen) and MutT-pcDNA3.1mycHis was verified by DNA sequencing. The MutT-MLS-myc (MutT-m) vector was generated by inserting the nucleotide sequence encoding the MLS from human Manganese Superoxide Dismutase (MnSOD) at the N terminus of MutT by using the forward primer 5'-TATAGGATCCACCATGTTGAGCCG GGCAGTGTGCGCACCCAGCAGGCAGCTGGCTCCGGCTTTGGGGATGAA AAAGCTGCAAATTCGGGTAGG-3' and the corresponding reverse complement primer as described for producing the MutT-MLS-myc vector.

The MUTYH-myc vector was generated by PCR amplification of MUTYH cDNA (GenBank accession number AF527839.1) using primers 5'-CCGGAATTCACC

ATGAGGAAGCCACGAGCAGCCGTG-3' and 5'-CCGCTCGAGCTACAGAT CCTCTTCTGAGATGAGTTTTTGTCTGGGCTGCACTGTTGAGGCTGT GT-3' with EcoRI restriction site in the forward primer and XhoI restriction site and myc tag in the reverse primer. The hOGG1-HA vector was generated by PCR amplification of OGG1 cDNA (GenBank accession number AB000410.1) using primers 5'-CCGGAATTCACCATGCCTGCCCGCGCTTCTGCC-3' and 5'-CCGCTCGAGTACCCATACGATGTTCCAGATTACGCTGCCTTCCGGCCC TTTGGAACCCCTT-3' with EcoRI restriction site in the forward primer and XhoI restriction site and HA tag in the reverse primer. Both inserts were restriction digested and ligated into pENTR4 (no ccdB) vector (Eric Campeau, Addgene plasmid 17424) and verified by sequencing. The entry clones were transferred to pLENTI-CMV/TO vectors (E. Campeau, Addgene plasmid 17292 and 17294) with zeocin and neomycin resistance using LR clonase (Invitrogen) reactions. The destination vectors were verified by sequencing.

**shRNA constructs.** To allow for easier cloning and use of shRNA constructs, the doxycycline-inducible lentiviral vector FH1tUTG was modified by replacing the GFP marker with a Puro cassette<sup>34</sup>. PCR products using BlnI-T2A-F and T2A-R primers on FH1tUTG plasmid and PURO-F and NotI-PURO-R primers on pMSCV-PURO plasmid (Clontech) were isolated and used in a subsequent PCR reaction to create the PCR fragment BlnI-T2A-Puro-NotI. This was recombined in a three-way ligation with NotI/NdeI and NdeI/BlnI fragments of FH1tUTG. Next, a PacI fragment was exchanged with a synthetic gene (DNA2.0) containing the following sequence: 5'-TTAATTAATAATTTGTCATGTCGCTAGTGTCTGGGAAA TCACCATAAACGTGAAATGCTTTGGATTGGGAATCTTATAAAGTCCC TATCAGTGATAGAGACTCGAGCCGAGAAATCTCTTACCTCAATTCAAG AGATTGAGGTAAGAGATTTCTCGGTTTTGAATTCGCGCGCTAGCCTG CAGGGGTCAATTAGTTCATAGCCCATATTAATTA-3'. Underlined sections of the sequence are the XhoI/EcoRI sites that are subsequently used to clone annealed oligonucleotides containing hairpins designed according to the following format, where the 21Ns contain the target sequence, or its reverse complement when underlined: forward primer 5'-TCGAGN<sub>21</sub>TTCAAGAGAN<sub>21</sub>TTTTTC-3', reverse primer 5'-AATTGAAAAAN<sub>21</sub>TCTCTTGAAN<sub>21</sub>C-3'.

Primers used: BlnI-T2A-F: 5'-GCTGAGCCTGCATTCCTTTTGGCCTGG AACTGA-3', T2A-R: 5'-CACCGTGGGCTGTACTCGGTCATTGGGCCAG GATTCTCTCGACG-3'; PURO-F: 5'-GTGACGTCGAGGAGAATCCTGGC CCAATGACCGAGTACAAGCCACCGGTG-3', NotI-PURO-R: 5'-GCGGCC GCTCAGGCCCGGCTTGGC-3'.

Target sequences: TP53 shRNA #d 5'-CACCATCCACTACAACACTACAT-3', TP53 shRNA #e 5'-GAGGGATGTTTGGGAGATGTA-3', MTH1 shRNA #2 5'-GAAAUUCCACGGGUACUUC-3', MTH1 shRNA #3 5'-CGACGACAGCUA CUGGUUU-3', NT shRNA 5'-GGAAGTACGATACGTAAGTAA-3'.

**Bacterial expression constructs.** The catalytically dead mutant, MTH1(E56A), was PCR amplified from the eukaryotic expression construct using the oligonucleotides MTH1 NdeIF: 5'-ATATCATATGGGCGCCTCCAGGCTCTATAC-3' and MTH1 NotIR: 5'-ATATGCGGCGCTTACTAGACCGTGTCCACCTCG-3'. The PCR product was digested with NdeI and NotI and subcloned into the bacterial expression vector pET28a(+) (Novagen). *E. coli* MutT cDNA was PCR amplified from the eukaryotic expression construct using the oligonucleotides MutTEcoli\_NdeIF: 5'-TATACATATGAAAAAGCTGCAAATTCGGGTAGG-3' and MutTEcoli\_SalIR: 5'-TATAGTCGACCTACAGACGTTAAGCTTCGCAATTAC-3', and ligated into pET28a(+) using the SalI and NdeI restriction sites.

**Expression and purification of MTH1 and MTH1 mutants.** A large-scale expression and purification of MTH1 (GenBank accession number D38594.2) wild type was performed as described previously<sup>19</sup>. His-tagged variants of MTH1 wild type and E56A were expressed from the pET28a(+) vector in *E. coli* BL21 DE3 (Life technologies). The proteins were purified from the bacterial lysate using MagneHis Ni-Particles (Promega). MagneHis beads were washed with buffer A (10 mM Tris-HCl pH 7.4, 1 mM DTT, 500 mM NaCl) and protein was eluted by buffer A fortified by 500 mM imidazole. Samples from the different purification steps were analysed using SDS-PAGE (Extended Data Fig. 2b). The concentrations of the purified proteins were determined by measuring A<sub>280</sub> and calculated using the extinction coefficient 28,000 M<sup>-1</sup> cm<sup>-1</sup>. The activity of His-tagged MTH1 wild type and E56A was tested with 100  $\mu$ M dGTP and normalized to nanomolar concentrations of enzyme (Extended Data Fig. 2c).

MTH1(D119A) and MTH1(W117Y) were expressed in *E. coli* BL21(DE3) R3 pRARE2 at 30 °C and purified on HisTrap HP column (GE Healthcare) followed by gel filtration on HiLoad 16/60 Superdex 75 (GE Healthcare); the His-tag was removed using thrombin digestion and the resulting untagged protein was further purified on a monoQ anion exchange column (GE Healthcare). The purity of 4  $\mu$ g of the protein preparations were checked on SDS-PAGE followed by Coomassie staining (Extended Data Fig. 2d).

**Expression and purification of *E. coli* MutT.** The pET28MutT construct was transformed into *E. coli* BL21DE3 pLysS, and MutT (GenBank accession number

X04831.1) was expressed at 18 °C and purified using a HisTrap column (GE Healthcare) following by removal of the His tag by thrombin digestion and further purification using the gel filtration column HiLoad 16/60 Superdex 75 (GE Healthcare). The purity of the protein preparation was checked on SDS-PAGE (Extended Data Fig. 3a) and mass spectrometry analysis and the concentration was determined by measuring  $A_{280}$  and the extinction coefficient  $28,990 \text{ M}^{-1} \text{ cm}^{-1}$ .

**Expression and purification of OGG1 and MUTYH.** Human *MUTYH* cDNA (GenBank accession number AF527839.1) was fused to *E. coli male* gene encoding the maltose-binding protein (MBP) in the pMal-c2x expression vector (New England Biolabs). The MBP-MUTYH fusion protein was expressed in *E. coli* strain BL21(DE3) pLysS at 25 °C and in presence of 75  $\mu\text{M}$  IPTG and purified using MBP-TrapHP and MonoQ anion exchange columns (GE Healthcare).

Human *OGG1* cDNA (GenBank accession number AB000410.1) was inserted into pNIC28-Bsa4 by ligation-independent cloning. *OGG1* expression in *E. coli* strain Rosetta2 (DE3) pLysS was induced by the addition of 0.5 mM IPTG and allowed to proceed for 18 h at 18 °C. His-tagged *OGG1* was purified by chromatography on HisTrap and SP cation exchange columns (GE Healthcare). The purity of the enzyme preparations were analysed on SDS-PAGE (Extended Data Fig. 2e, f).

**Transfections.** For siRNA transfections, cells were seeded at 20–40% confluency and the day after transfected with 10 nM siRNA and INTERFERin (Polyplus Transfections) according to the manufacturer's protocol. Cells were transfected in media without PeSt. For NT RNA control, the All-stars negative control (Qiagen) was used. The following siRNA sequences were used: MTH1 siRNA #1 GACGACAG CUACUGGUUUC; MTH1 siRNA #2 GAAAUUCCACGGGUACUUC; MTH1 siRNA #3 CGACGACAGCUACUGGUUU.

Stable cell lines were made by transfecting cells with plasmid DNA and JetPEI (Polyplus Transfections) according to the manufacturer's protocol. Cells that had integrated the plasmid DNA in their genome were selected using 2  $\mu\text{g ml}^{-1}$  puromycin (MTH1-puro vector) or 400  $\mu\text{g ml}^{-1}$  G418 (MutT-*myc* vector) for 2 weeks before single cell clones were isolated. Overexpression was verified by western blot analysis.

**Virus production.** Lentiviral infections were made by calcium-phosphate-mediated co-transfection of HEK 293T cells with packaging plasmids plus one of either four different shRNA constructs directed against MTH1 or two shRNA constructs directed against p53 (see above DNA plasmids). 24 h after transfection the different supernatants were collected two times with 24-h intervals, filtered and then used to infect U2OS and SW480 cells grown under optimal conditions. The cells were selected by culturing in the presence of 2  $\mu\text{g ml}^{-1}$  puromycin for 72 h or until all control cells were completely dead.

**Clonogenic outgrowth assay.** For siRNA experiments, cells were seeded at approximately 30% confluency in 6-well plates in complete medium. The day after, the medium was aspirated and fresh medium without antibiotics was added. The cells were transfected and/or treated with doxycycline (2  $\mu\text{g ml}^{-1}$ ). On day 5, cells were either trypsinized, counted and re-seeded for clonogenic outgrowth on 10-cm plates with 500 cells per plate, or analysed by western blotting. After additional 7–10 days, plates were fixed and stained with 4% methylene blue in MeOH and colonies counted manually.

For MTH1 inhibitor experiments, cells were seeded for clonogenic outgrowth on 10-cm plates with 500 cells per plate. After 5 h of incubation (5%  $\text{CO}_2$  at 37 °C) cells were treated with vehicle (maximum 0.2% DMSO) or compound at various concentrations. After 7–14 days, plates were fixed and stained with 4% methylene blue in MeOH and colonies counted manually.

**Calcein AM viability assay.** Cells were seeded in 96-well plates (3,000 cells per well) and the day after treated with compounds or vehicle. After 72 h, cells were washed three times with PBS and incubated with 1  $\mu\text{M}$  calcein AM (CalbioChem) for 30 min at room temperature. Fluorescence was measured at 495/520 nm (ex/em).

**Resazurin viability assay.** Cells were seeded into 96-well plates (1,500 cells per well) and the day after treated with compound or vehicle (maximum 0.2% DMSO). After 72 h cells were stained with resazurin. Fluorescence intensity was measured at 530/590 nm (ex/em) after 2 h incubation with resazurin<sup>35</sup>.  $\text{IC}_{50}$  values were calculated using GraphPad Prism Software Inc., nonlinear curve fit with variable slope (four parameters).

**Caspase 3 apoptosis assay.** U2OS cells were seeded in a 24-well plate (50,000 cells per well). The following day, cells were treated with MTH1 inhibitors with concentrations ranging from 0.5 to 10  $\mu\text{M}$  or vehicle (DMSO 0.1%). After 72 h the supernatant and trypsinized cells were collected as a single cell suspension, spun down, and later washed in PBS. The cells were fixed in 4% PFA for 10 min at room temperature, washed once in PBS and permeabilized by a 30-min incubation on ice in 90% ice-cold MeOH. 0.5% BSA/PBS was added at a ratio of 2:1 to the MeOH and spun down. The cells were washed in 0.5% BSA/PBS, spun down and blocked in 0.5% BSA/PBS for 10 min at room temperature, followed by 1 h incubation at room temperature with cleaved caspase 3 antibody (Cell Signaling Ab 9661) in 0.5% BSA/PBS at a concentration of 1:2,000. After additional washing, the cell

pellet was re-suspended in 0.5% BSA/PBS containing Alexa 488 donkey-anti rabbit IgG at a concentration of 1:500 (Invitrogen, A-21206) and incubated for 30 min at room temperature in the dark. After an additional two washes, the cell pellet was re-suspended in 0.5% BSA/PBS containing 50  $\mu\text{g ml}^{-1}$  propidium iodide (Sigma Aldrich) and 20  $\mu\text{g ml}^{-1}$  of RNase (Fermentas) and incubated at 4 °C for 30 min. The samples were analysed on a BD FACScalibur. The SubG1 fraction (apoptotic) was analysed in the FL2 channel, where two log scales below the G1 population was scored as apoptotic. For cleaved caspase 3 (FL1 channel), only signal in the viable cell population (G1, S and G2/M as scored by PI histograms in a linear FL3 channel) was gated as positive.

**Immunofluorescence.** For confocal microscopy, cells were seeded on coverslips in 24-well plates (10,000–15,000 cells per well). The next day, the cells were transfected with siRNA and after 72 h the medium was changed to fresh medium. For the p53 shRNA experiments, 2  $\mu\text{g ml}^{-1}$  doxycycline was added during the whole experiment. For the EdU experiments, 10  $\mu\text{g ml}^{-1}$  EdU (Invitrogen) was added and cells were incubated for 15 min at 37 °C. Cells were fixed with 3% paraformaldehyde in PBS pH 7.5 with 0.1% Triton X-100 for 15 min at room temperature. Samples were permeabilized with 0.3% Triton X-100 in PBS and blocked in 3% BSA, 0.1% Tween 20 in PBS. Primary and secondary Alexa-Fluor-conjugated antibodies were diluted in 3% BSA, 0.1% Tween 20 in PBS. DNA was counterstained with To-Pro3 (Invitrogen). Images were acquired in a Zeiss LSM-510 confocal microscope with the 63 $\times$  oil objective.

For high-throughput immunofluorescence, cells were seeded in 96-well plates (2,500–3,000 cells per well). The day after, cells were either transfected with siRNA or treated with compounds. Cells were fixed and stained as described above. DNA was counterstained with DAPI.

Quantification was either done by manual counting of positive cells in the microscope ( $n > 200$  cells per sample) or by automatic acquisition of images ( $n > 500$  cells per well) using the In Cell Analyzer 2000 (GE Healthcare) and Developer software (GE Healthcare).

**Western blot assay.** Cells were grown in 6-well plates, washed with PBS and scraped in lysis buffer (10 mM HEPES pH 7.1, 50 mM NaCl, 0.3 M sucrose, 0.1 mM EDTA, 0.5% Triton X-100, 1 mM DTT and 1 $\times$  protease inhibitor cocktail (Pierce)). Samples were kept on ice for 15 min after which 4 $\times$  sample buffer (Invitrogen) was added and samples were denatured at 95 °C for 10 min. Proteins were separated on 4–12% Bis-Tris acrylamide gels/1 $\times$  MES running buffer (Invitrogen). After separation, proteins were transferred to Hybond ECL nitrocellulose membranes (GE Healthcare) followed by blocking with 5% milk/1% BSA in TBS-Tween 20. Blots were probed with primary and HRP-conjugated secondary antibodies and developed with SuperSignal West Femto substrate (Pierce).

**8-oxo-dG assay.** Avidin has previously been shown to bind with high specificity to 8-oxodG<sup>36</sup> and was therefore used for the 8-oxodG measurements. Cells were fixed in pure methanol at –20 °C for 20 min and thereafter incubated for 15 min in TBS with 0.1% Triton X-100. Blocking was accomplished in 15% FBS, 0.1% Triton X-100 in TBS for 2 h in room temperature. Cells were then incubated with 10  $\mu\text{g ml}^{-1}$  Alexa488-conjugated avidin (Invitrogen) in blocking solution for 1 h at 37 °C to subsequently be rinsed in TBS with 0.1% Triton X-100 for 2  $\times$  5 min at room temperature. After a quick rinse in distilled water, DNA was counterstained with ToPro3-Iodide (LifeTechnologies) for 15 min at room temperature. Finally the plates were rinsed in TBS.

For the 96-well experiments, 1,500 cells were seeded in each well the day before siRNA transfection or treatment with inhibitors. Three days after beginning of inhibitor treatment, or 5 days after transfection, cells were fixed and stained as described above.

For confocal microscopy, 10,000 cells were seeded on round coverslips in 12-well plates the day before siRNA transfection. The cells were seeded in a rod-like pattern on the coverslip to get room for cell expansion. Five days after transfection cells were fixed and stained as described above. Coverslips were mounted with ProLongGold (Invitrogen) and images were acquired from the rim of the cell layer with a Zeiss LCM 510-inverted microscope using a planapochromat 63 $\times$ , NA 1.4 oil immersion objective. Images were analysed automatically, with a program written in-house using NIH-imageJ, with respect to mean intensity in the nucleus (To-Pro3 was used as DNA marker).

**Comet assay.** For siRNA experiments, U2OS cells were seeded in 6-well plates (70,000 cells per well) and transfected with non-targeting (NT) siRNA or MTH1 siRNA #1. After 5 days, cells were harvested by trypsinization. For small molecule experiments, U2OS cells or VH10 cells were seeded in 6-well plates (150,000 cells per well) and treated with 10  $\mu\text{M}$  MTH1 inhibitor for 24 h before harvesting or with 100  $\mu\text{M}$   $\text{H}_2\text{O}_2$  for 5 min on ice. Cells were harvested as above. After washing with 1 $\times$  PBS, cells were re-suspended in 1 $\times$  PBS at a concentration of approximately  $1 \times 10^6$  cells  $\text{ml}^{-1}$ . 50  $\mu\text{l}$  cell suspension was mixed with 250  $\mu\text{l}$  1.2% low-melting agarose at 37 °C. The mixture was added to pre-warmed (37 °C) agarose coated fully frosted slides (Thermo-Fisher Scientific) and a coverslip was added

on top of the mixture. The slides were kept on ice for 10 min before removing the coverslip and incubated in lysis buffer (10 mM Tris pH 10.0, 2.5 M NaCl, 0.1 M EDTA, 10% DMSO and 1% Triton X-100) at 4 °C overnight in the dark. Slides were washed three times with enzyme reaction buffer (40 mM HEPES pH 8.0, 0.1 M KCl, 0.5 mM EDTA and 0.2 mg ml<sup>-1</sup> BSA) and incubated with buffer alone, OGG1 (1.0 µg ml<sup>-1</sup>) or MUTYH (1.2 µg ml<sup>-1</sup>) at 37 °C for 45 min. Slides were washed once with enzyme reaction buffer and incubated in alkaline electrophoresis buffer (0.3 N NaOH, 1 mM EDTA) for 30 min. Electrophoresis was run at 300 mA, 25 V for 30 min in electrophoresis buffer using a Comet Assay tank (Thistle Scientific). Slides were washed in neutralization buffer (0.4 M Tris-HCl pH 7.5) and counterstained with 5 µM YOYO-1 dye (Invitrogen). Images were acquired with a 20× or 10× objective in a Zeiss LSM 510 confocal microscope and quantified using CometScore software. At least 100 comets per sample were analysed. Tail moment is calculated as per cent DNA in the tail multiplied by the tail length.

**Determination of carbonylated proteins.** Carbonylated proteins were measured following established protocols<sup>37</sup>. In brief, cells were washed with ice-cold PBS and rapidly lysed in ice-cold lysis buffer. Subsequently, DNA was removed with streptomycin sulphate and 2,4-diphenylhydrazine was added to a final concentration of 2 mM. After incubation, proteins were precipitated with trichloroacetic acid, washed with ethanol/ethylacetate three times and dissolved in 6 M guanidinium hydrochloride. Absorbance was measured at 366 nm and normalized to protein content.

**Compound libraries.** Screening for inhibitors of MTH1 was done at the Laboratories of Chemical Biology Karolinska Institutet (LCBKI), part of Chemical Biology Consortium Sweden, and at the RNAi Cell screening Facility, SciLifeLab Stockholm using a compound concentration of 10 µM in 96- and 384-well microtitre plate based assays. Compounds originating from Enamine, ChemDiv, Timtec and Maybridge along with LCBKI in-house compound library (donated by Biovitrum AB) were screened. For the 384-well-based assay, all assay plates contained test compounds in columns 1–22, whereas negative and positive controls in column 23 and column 24 were used for normalization. In this layout the negative controls represent the uninhibited enzyme, corresponding to empty wells or wells with the equivalent amount of DMSO as the compound containing wells, whereas the positive controls represent the completely inhibited enzyme, corresponding to the lack of MTH1.

**Screening assay.** The enzymatic assay applied for screening purposes was based on the enzymatic hydrolysis of dGTP by purified human recombinant MTH1 to form dGMP and pyrophosphate. An excess of inorganic pyrophosphatase was added to the assay, which allows the quantification of released inorganic phosphate as a measure of product levels in a coupled enzymatic assay. Inorganic phosphate was measured using an absorbance assay based on malachite green, as previously described<sup>38</sup>. The assay buffer in which MTH1, inorganic pyrophosphatase and dGTP were diluted consisted of 100 mM Tris-acetate at pH 8.0, 40 mM NaCl, 10 mM Mg acetate, 0.005% Tween 20 and 1 mM DTT. The final conditions in the assay during enzymatic incubation were 0.5–2 nM recombinant human MTH1, 100 µM dGTP and 0.2 U ml<sup>-1</sup> inorganic pyrophosphatase. The assay volumes were 100 µl and 40 µl in the 96-well and 384-well based assays, respectively. An Echo 550 (Labcyte) was used for dispensing of compound solutions, whereas a FlexDrop (PerkinElmer) was used for dispensing of enzyme and substrate solutions. After incubation of enzymes and substrate at room temperature for 1 h, the reaction was terminated and the signal developed by the addition of the malachite green reagent using a MultiDrop (Thermo Scientific). After shaking and colour development for a minimum of 15 min the plates were analysed in a microplate reader using a filter at 630 nm (Victor 2 and 3 instruments from PerkinElmer).

**IC<sub>50</sub> value determination.** For IC<sub>50</sub> value determination the screening assay described above was slightly modified. Briefly, the compounds to be analysed were first serially diluted in DMSO in a 1:3 dilution series and then further diluted in assay buffer (100 mM Tris-acetate, 40 mM NaCl, 10 mM Mg acetate, 1 mM DTT and 0.005% Tween 20) generating 11 different compound concentrations giving a final DMSO concentration of 1% in the assay well. MTH1 was added to a final concentration of 4.8 nM. dGTP was added to a final concentration of 100 µM and 0.2 U ml<sup>-1</sup> inorganic pyrophosphatase was added to a final volume of 100 µl. A dilution series of a QC substance was included on each assay plate as well as controls lacking enzyme (negative control) or inhibitor (positive control). The reaction mixture was incubated with shaking for 15 min at 22 °C. 25 µl malachite green assay reagent was added followed by incubation with shaking for 15 min at 22 °C. The absorbance of the assay plate was read at 630 nm using an EnVision Multilabel plate reader. The IC<sub>50</sub> value was determined by fitting a dose response curve to the data points using nonlinear regression analysis and the equation  $Y = Y_{\min} + (Y_{\max} - Y_{\min}) / (1 + 10^{(\log(\text{IC}_{50} - X) \times \text{HillSlope}))}$ , where  $Y$  is the read absorbance at 630 nm and  $X$  is  $\log[\text{compound}]$ . For the most potent compounds the enzymatic assay reached its limit in terms of potency resolution due to tight binding

conditions. Therefore, a more sensitive assay was developed with a final MTH1 concentration of 0.2 nM and a reaction time of 8 h.

**MutT activity assay and inhibition by MTH1 inhibitors.** The developed MTH1 assay described above was optimized for MutT (GenBank accession number X04831.1) with respect to reaction time and enzyme concentration. Inhibition of *E. coli* MutT by MTH1 inhibitors was studied by measuring the enzymatic activity of 9.6 nM *E. coli* MutT with 100 µM dGTP in MTH1 assay buffer in the presence of various concentrations of the inhibitors as described above for MTH1. Inhibition experiments of MTH1 with the same inhibitor dilutions were performed in parallel.

**Inhibition analysis using 2-OH-dATP and 8-oxodGTP as substrates.** MTH1 activity assay conditions were 0.5 nM MTH1, 8.3 µM 2-OH-dATP (Jena Bioscience) and 13.2 µM for 8-oxodGTP (Trilink Biotechnologies), the respective  $K_m$  values for these substrates, in MTH1 reaction buffer (10 mM Tris-acetate pH 7.5, 40 mM NaCl, 10 mM Mg acetate, 1 mM DTT and 0.005% Tween 20). After a reaction time of 30 min, released PPi was detected using the PPiLight inorganic pyrophosphate assay kit from Lonza and luminescence was monitored using Mithras<sup>2</sup> LB 943 Multimode reader (Berthold Technologies). Dose-response curves using TH287 concentrations ranging from 1 µM to 2 pM and TH588 concentrations ranging from 3 µM to 6 pM in 1:3 serial dilution steps were recorded. IC<sub>50</sub> values were determined using nonlinear regression and the GraphPad Prism software.

**Activity assessment of MTH1(D119A) and MTH1(W117Y).** The activity of wild-type MTH1, MTH1(D119A) and MTH1(W117Y) with 20 µM 8-oxodGTP and 20 µM 2-OH-dATP was assayed in MTH1 reaction buffer using 1 nM enzyme. After a 30 min reaction, released PPi was detected using the PPiLight Inorganic Pyrophosphate Assay (Lonza). A standard curve of PPi between 0–5 µM was used to determine how much substrate was converted to product. Activity of the two mutants relative to wild type was determined.

**Selectivity assays.** His-tagged NUDIX superfamily enzymes MTH2 (GenBank accession number BC133017.1), NUDT12 (GenBank accession number BC041099.1), NUDT14 (GenBank accession number NM\_177533.4) and NUDT16 (GenBank accession number BC031215.1) and the pyrophosphate hydrolase enzyme ITPase (GenBank accession number AF219116.1) were expressed from the bacterial expression vector pNIC28-Bsa4 and purified by the Protein Science Facility (PSF) at Karolinska Institutet using HisTrap HP (GE Healthcare) followed by gel filtration on HiLoad 16/60 Superdex 75 (GE Healthcare). NUDT5 (GenBank accession number BC000025.2) was expressed from pNIC28-Bsa4 and purified in-house using a HisTrap HP column followed by removal of the His-tag by TEV protease digestion and further purification on MonoQ ion exchange column (GE Healthcare). Human dCTPase (GenBank accession number NM\_024096.1) and dUTPase (GenBank accession number AF018429.1) were expressed as His-tagged proteins from the pET28a(+) vector and purified on HisTrap HP. The His-tag was removed from dUTPase by thrombin digestion and from dCTPase by TEV digestion. The proteins were further purified using a MonoQ ion exchange column. The purity of all the protein preparations used was checked by SDS-PAGE followed by Coomassie staining (Extended Data Fig. 8h).

Enzymatic activity assays were developed for MTH2, NUDT5, NUDT12, NUDT14, NUDT16, dCTPase, dUTPase and ITPA. All assays were run in MTH1 reaction buffer (10 mM Tris-acetate pH 7.5, 40 mM NaCl, 10 mM Mg acetate, 1 mM DTT and 0.005% Tween 20) with the modifications indicated below. The reactions were coupled to pyrophosphatase (PPase) or calf intestinal phosphatase (CIP) to produce inorganic phosphate that can be detected by using the malachite green reagent. The assay conditions were for MTH2: 0.2 U ml<sup>-1</sup> PPase, 100 µM dGTP and 8 nM MTH2; for NUDT5, NUDT12 and NUDT14: 2.5 U ml<sup>-1</sup> CIP, 50 µM ADP ribose and 6 nM NUDT5, 200 nM NUDT12 and 2 nM NUDT14, respectively; for NUDT16: 0.2 U ml<sup>-1</sup> PPase, 50 µM ITP and 1,000 nM NUDT16. The assay conditions were for dCTPase: 0.2 U ml<sup>-1</sup> PPase, 35 µM dCTP and 35 nM dCTPase in MTH1 reaction buffer containing 100 mM NaCl; for dUTPase: 0.2 U ml<sup>-1</sup> PPase, 12.5 µM dUTP and 1 nM dUTPase; for ITPA: 0.2 U ml<sup>-1</sup> PPase, 25 µM ITP and 0.1 nM ITPA in MTH1 reaction buffer lacking NaCl and fortified with 50 mM MgAc. The compounds TH287, TH588 and TH650 were tested against these targets as described for MTH1 above. The target substrate concentrations were set at  $K_m$ .

TH588 (10 µM) was tested at CEREP (France) in their High-Throughput Profile and hERG assay with additional assay for ALK.

**Isothermal titration calorimetry.** MTH1 samples intended for isothermal titration calorimetry (ITC) experiments were dialysed in ice-cold buffer (100 mM Tris-acetate, 40 mM NaCl, 10 mM MgCl<sub>2</sub>, 0.005% Tween-20 and 1 mM DTT at pH 7.9 when measured at room temperature). Compounds were diluted from DMSO stock solutions in the dialysis buffer and the corresponding amount of DMSO was also added to the dialysed MTH1 samples to ensure the buffers matched. All experiments were performed on a MicroCal Auto-iTC<sub>200</sub> instrument (GE Healthcare) with the experimental temperature at 25 °C and data analysis was achieved using the Origin 7.0 software for the iTC<sub>200</sub>. Besides the titrations of compounds into MTH1 samples we performed control titrations of compound into dialysis buffer,

which resulted in similar-sized peaks as those seen towards the end of the compound titrations when MTH1 was saturated with compound. A constant small value was therefore subtracted from the data to remove this background before fitting the binding isotherms. All data could be fitted using the one-site model within the Origin software and resulted in best-fit parameters for the association constant ( $K$ ), the enthalpy of binding ( $\Delta H$ ) and the apparent stoichiometry ( $n$ ). It should be noted that some of the curves gave steep binding isotherms with very high  $C$  values (Extended Data Fig. 3f), such that the data are better used as confirmatory of the potent binding, as observed in the enzymatic assay, rather than precise quantitative estimates of the affinities.

**Target engagement assay.** Target engagement in cells was evaluated using the general principles of the method described previously<sup>18</sup>. In brief, BJ SV40T RasV12-cells were seeded into T225 culture flasks. After 24 h, the cells were treated with 1% DMSO in cell media or 50  $\mu\text{M}$  TH287, TH588 or TH650 for 3–5 h. Cells were harvested using trypsin, spun down and subsequently re-suspended in TBS. The cell suspension was aliquoted into 12 PCR tubes and heated for 3 min to 42, 44, 46, 48, 50, 52, 54, 56, 58 or 60 °C. Cells were lysed by three repeated cycles of freeze-thawing, using ethanol on dry ice. The precipitated proteins were separated from the soluble fraction by centrifugation at 17,000g for 20 min. Supernatants were kept at –80 °C until western blot analysis. One-fifth of each aliquot was loaded onto 4–25% SDS-PAGE gels, blotted on nitrocellulose membranes and analysed for MTH1 content using the MTH1 antibody from Novus Biologicals at a concentration of 1:500.

**Surface plasmon resonance analysis.** Surface plasmon resonance analysis was carried out on the Biacore T200 instrument. Purified MTH1 protein was immobilized on CM5 chip, using amine coupling according to the supplier's (GE Healthcare Lifesciences) instruction, to obtain immobilization levels around 1,300 RU. Inhibitors were screened at five different concentrations at a DMSO concentration of 5% in a running buffer composed of 100 mM Tris-acetate, 10 mM Mg acetate, 40 mM NaCl and 0.05% Tween 20. Solvent correction, blank subtraction and exclusion of responses caused by buffer changes preceded the analysis of on-rate, dissociation rate and affinity. The experiment was repeated on three different occasions.

**Synthesis of MTH1 inhibitors.** All reagents were commercial grade and used without further purification. Flash column chromatography was performed on Merck silica gel 60 (70–230 mesh). Preparative HPLC was performed on a Gilson HPLC system: Column ACE 5 C8 (150  $\times$  30 mm); H<sub>2</sub>O (containing 0.1% TFA) and MeCN were used as mobile phases. Analytical LCMS was conducted using an Agilent MSD mass spectrometer connected to an Agilent 1100 HPLC. System A: Column ACE 3 C8 (50  $\times$  3.0 mm); H<sub>2</sub>O (+ 0.1% TFA) and MeCN were used as mobile phases; system B: Xterra MS C18 (50  $\times$  3.0 mm); H<sub>2</sub>O (containing 10 mM NH<sub>4</sub>HCO<sub>3</sub>; pH = 10) and MeCN were used as mobile phases. All compounds gave satisfactory purities when analysed using both systems. <sup>1</sup>H NMR spectra were recorded on a Bruker Advance DPX 400 spectrometer at 400.1 MHz. High-resolution mass spectra (HRMS) were collected on a Maxis Impact ToF mass spectrometer. Instant JChem was used for structure and reagent database management, Instant JChem 6.1.0, 2013, ChemAxon (<http://www.chemaxon.com>). Of the MTH1 inhibitors described N<sup>4</sup>-methyl-6-phenylpyrimidine-2,4-diamine (TH086) has previously been described<sup>39</sup>. Synthesis and analysis of all other compounds is detailed in the Supplementary Information.

**Co-crystallization.** 3 mM TH287 or 5 mM TH588, 6 mM MgCl<sub>2</sub> and 2 mM TCEP was added to MTH1. Sitting-drop vapour diffusion experiments at 18 °C were performed, and MTH1 (11–13 mg ml<sup>-1</sup>) was mixed with reservoir solution (22–32% PEG6000, 0.1 M sodium acetate pH 3.5 and 0.2 M LiSO<sub>4</sub>) in a 1:1 ratio. Diffraction quality crystals appeared after about 5 days, were cryo-protected by soaking them in mother liquor supplemented with 15% glycerol, and were subsequently flash-frozen in liquid nitrogen. Data collection was performed beamline 14.1 at BESSY, Germany, at 100 K. Data reduction and processing was carried out using XDS<sup>40</sup> and programs from the CCP4 suite (Collaborative Computational Project 4, 1994). Relevant statistics can be found in Supplementary Table 1. The structure was solved via molecular replacement, using the previously solved *apo* MTH1 structure as search model (Protein Data Bank code 3ZR1). A few cycles of refinement in Refmac<sup>41</sup>, interspersed with manual building in Coot<sup>42</sup>, were needed to complete the model. Water molecules were automatically placed in the maps, using a  $F_{\text{O}} - F_{\text{C}}$  Fourier difference map cutoff of 3 $\sigma$ , and were subsequently validated to ensure correct positioning. The final protein model contains residues 3–156 (MTH1: TH287) and 2–155 (MTH1:TH588). All structure figures were prepared using PyMOL. Ramachandran statistics were generated using MolProbity. The structure has been deposited in the Protein Data Bank with accession code 4N1T (MTH1 with TH287) and 4N1U (MTH1 with TH588).

**In vitro ADME solubility assay.** The solubility assay of the MTH1 inhibitor compounds was performed by addition of 1  $\mu\text{l}$  of 10 mM DMSO stock solution to 100  $\mu\text{l}$  of PBS. The samples were incubated at 37 °C for 2 h in sealed glass vials and analysed by liquid chromatography-mass spectrometry (LC-MS/MS).

**In vitro ADME plasma protein binding assay.** Pooled human plasma was provided by Uppsala Academic Hospital and was collected from two male and two female donors (non-smoking). The assay was performed using Rapid Equilibrium Dialysis (RED) device (Thermo Scientific) as described previously<sup>43</sup>. The plasma test solution was spiked with test compound to a final concentration of 10  $\mu\text{M}$  (from a 10 mM DMSO stock) and dialysed against PBS pH 7.4. In addition, a separate stability test was performed (to allow detection of plasma drug degradation) and was incubated at 37 °C for 4 h. After the incubation, the contents of each plasma, stability and buffer compartment were removed and mixed with equal volumes of control buffer or plasma as appropriate to maintain matrix composition for analysis. Plasma proteins were precipitated by ice-cold methanol (1:4) containing warfarin as analytical internal standard. The samples were centrifuged and the supernatant was analysed by mass spectrometry (LC-MS/MS).

**Calculations.** The unbound fraction of candidate drug was determined using the relationship in equation (1), where plasma concentration and free concentration were the concentrations obtained from LC-MS/MS analysis of the plasma and buffer compartments, respectively.

$$f_u = \frac{C_{\text{unbound}}}{C_{\text{total}}} = \frac{C_{\text{buffer,dialysate}}}{C_{\text{plasma,dialysate}}} \quad (1)$$

**In vitro ADME metabolic stability assay.** The MTH1 inhibitors at a final concentration of 1  $\mu\text{M}$  were incubated in the presence of 0.5 mg ml<sup>-1</sup> pooled human (CellzDirect Inc.) or pooled mouse CD-1 liver microsomes (XenoTech LLC) in 100 mM K phosphate buffer pH 7.4. The reaction was initiated by addition of NADPH to a final concentration of 1 mM. The incubation times were 0, 5, 15, 40 min (duplicate) and the reaction was quenched, at each time point, by addition of 100  $\mu\text{l}$  ice-cold acetonitrile. Precipitated proteins were removed by centrifugation at 3,500 r.p.m. for 20 min at 4 °C before LC-MS/MS analysis. Midazolam and dextromethorphan were used to test for the microsomal CYP control activity at each experimental occasion.

The calculations of *in vitro* half-life ( $T_{1/2}$ ), intrinsic clearance ( $CL_{\text{int}}$ ) and predicted hepatic extraction ratio ( $E$ ) were performed as described previously<sup>44,45</sup>.

**In vitro ADME metabolite identification assay.** The incubations for determination of TH287 and TH588 metabolites were performed at 37 °C with 1 mg ml<sup>-1</sup> of mouse or human microsomal proteins and 1 mM NADPH in a total volume of 100  $\mu\text{l}$  of 100 mM K phosphate buffer pH 7.4. The compounds were incubated at a final concentration of 10  $\mu\text{M}$  and the reaction was terminated after 60 min with ice-cold acetonitrile. Precipitated proteins were removed by centrifugation at 3,500 r.p.m. for 20 min at 4 °C. The control reaction was precipitated before addition of the test compounds and was incubated for the same period of time.

**In vitro ADME Caco-2 permeability assay.** The Caco-2 study was performed in accordance with published protocols<sup>46</sup>. Caco-2 cell monolayers (passage 94-105) were grown on permeable filter supports and used for transport studies on day 21 after seeding. Before the experiment a drug solution of 10  $\mu\text{M}$  was prepared and warmed to 37 °C. The Caco-2 filters were washed with pre-warmed HBSS before the experiment, and thereafter the experiment was started by applying the donor solution on the apical or basolateral side of the cell monolayers. The transport experiments were carried out at pH 7.4 reflecting the pH of the blood. The experiments were performed at 37 °C and at a stirring rate of 500 r.p.m. The receiver compartment was sampled at 15, 30 and 60 min, and at 60 min also a final sample from the donor chamber was taken to calculate the mass balance of the compound.

Directly after the termination of the experiment the filter inserts were washed with pre-warmed HBSS and the membrane integrity was checked by trans-epithelial electrical resistance (TEER) measurement and by determination of <sup>14</sup>C-mannitol permeability (a paracellular marker used for integrity measurements).

**Calculations.** The permeability values were calculated from

$$C_{\text{R}}(t) = \frac{M}{V_{\text{D}} + V_{\text{R}}} + (C_{\text{R}(0)} - (M/(V_{\text{D}} + V_{\text{R}})))e^{-P_{\text{app}}A\left(\frac{1}{V_{\text{D}}} + \frac{1}{V_{\text{R}}}\right)t}$$

where  $C_{\text{R}}(t)$  is the time-dependent drug concentration in the receiver compartment,  $M$  is the amount of drug in the system,  $C_{\text{R},0}$  is the concentration in the receiver compartment at the start of the experiment,  $V_{\text{D}}$  and  $V_{\text{R}}$  are the volumes of the donor and receiver compartment, respectively,  $A$  is the surface area of the filter (cm<sup>2</sup>),  $t$  is the time from the start of the interval, and  $P_{\text{app}}$  is the apparent permeability coefficient (10<sup>-6</sup>  $\times$  cm s<sup>-1</sup>).

**In vitro ADME LC-MS/MS analysis.** All samples from the assays described above were analysed by LC-MS/MS. The following system was used: Waters XEVO TQ triple-quadrupole mass spectrometer (electrospray ionization, ESI) coupled to a Waters Acquity UPLC system (Waters Corp.). For chromatographic separation a general gradient was used (1% mobile phase B to 90% over 2 min total run) on a C18 BEH 1.7  $\mu\text{m}$  column 2  $\times$  50 mm (Waters Corp.). Mobile phase A consisted of

5% acetonitrile 0.1% formic acid and mobile phase B 100% acetonitrile 0.1% formic acid. The flow rate was 0.5 ml min<sup>-1</sup>. 5 µl of the sample were injected on a 10 µl loop (partial injection mode).

The samples for metabolite identification were analysed using a 5-min gradient (1% mobile phase B to 90%) and in full scan mode.

**Animals and pharmacokinetic and efficacy studies.** The animal experiments described here were approved (#N584/11, N2/11) by the regional animal ethical committee in Stockholm in compliance with EU 2010/63 directive. All animals were acclimatized for 1 week, and had free access to water and food as well as enrichment during the experiment. Animals were under a 12-h light cycle, and the temperature and the humidity according to laboratory animal guidelines and regulations. The animals were housed 3–5 mice per cage and cage size was according to laboratory animal guidelines and regulations. The group size was based on results from pilot studies and experience from the models on variations within the control group. Animals were randomized into the groups based on body weight (mean body weight of approximately 19 g, see figures for detailed information). In the pre-established tumour model, animals were grouped based on both body weight and tumour size; with a body weight mean of approximately 19 g and tumour volume of 70 mm<sup>3</sup> (see Extended Data Fig. 4 for details). The exclusion/inclusion criteria were predefined in the ethical permit. The experimenter was blinded when assessing the tumour volume. For statistical analysis, two-way analysis of variances (ANOVA) (GraphPad Prism 4.0, GraphPad Software Inc.) and pair-wise Bonferroni corrected comparisons between groups were used. Tumour volume and body weight were analysed using general linear model with repeated measures with experiment groups (treatment, control) as between-subject factors and day as within-subject factor. Significant interaction effects were analysed further with Sidak's post-hoc tests. For pharmacokinetic studies, C57BL/6 mice (female, 6–8 weeks at arrival, Scanbur, Germany, *n* = 12 per group) and SCID mice (female, 6–8 weeks, local breeder at Karolinska Institutet, Sweden) were used. Compound was administered subcutaneously (s.c., 10 ml kg<sup>-1</sup>) and blood samples were collected at various time points as noted in Extended Data Fig. 4 (blood sample from 3 mice per time point). For shRNA studies, SCID mice (*n* = 5 per group study 1 and *n* = 7 per group study 2, female, 5–6 weeks, local breeder at Karolinska Institutet, Sweden and Scanbur, Germany) were used. The study was repeated in two individual experiments. 1 × 10<sup>6</sup> cells were diluted in Matrigel (1:1, BD Biosciences) and injected subcutaneously in the sacral area. Tumour progression was monitored twice weekly. At a tumour size of 250 mm<sup>3</sup>, doxycycline was introduced into the drinking water (2 mg ml<sup>-1</sup>) to suppress MTH1 protein. At a tumour size of 1,000 mm<sup>3</sup> animals were euthanized. For the SW480 xenograft cancer model, SCID mice (*n* = 8 per group, female, 5–6 weeks, Scanbur, Germany) were used. 1 × 10<sup>6</sup> SW480 cells were diluted in Matrigel (1:1) and injected subcutaneously in the sacral area. Treatment was initiated one day after cell inoculation. For the MCF-7 xenograft cancer model in SCID mice (*n* = 10 per group, female, 5–6 weeks, Scanbur, Germany), an oestrogen pellet (E2 pellet, 21 days release, Innovative research) was implanted under anaesthesia. On the second day after receiving E2 pellet, 2 × 10<sup>6</sup> of MCF-7 cells were injected into the right flank to develop orthotopic breast cancer tumour. Treatment was initiated 8 days after cell inoculation when tumours reached an approximate size of 70 mm<sup>3</sup>. Vehicle or MTH1 inhibitor was administered subcutaneously for 35 days in SW480 xenograft study and 7 days in MCF-7 xenograft study. MTH1 inhibitor was diluted in 2% DMSO, 10% ethanol, 10% cremaphore, 10% Tween 80, 68% PBS. Tumour size was measured twice weekly (calculated as length × width × width × 0.52) and mice were weighed at least once weekly. At termination, blood was collected by orbital bleeding under anaesthesia and whole blood used for haematological analysis and EDTA collected plasma for ASAT, ALAT, creatinine analysis by the Karolinska Universitetslaboratoriet, Clinical Chemistry. A gross post-mortem inspection was performed. Tumours from SW480 xenograft model were fixed in paraformaldehyde (4%), embedded in paraffin and finally sectioned. Deparaffinization and rehydration of the sections were conducted before antigen retrieval in citrate buffer, in a pressure cooker. The sections were blocked for 2 h in 3% BSA before incubation with the primary antibodies CD31 and Ki67 (1:500 anti-PECAM-1 M20, SantaCruz, 1:500 anti-Ki67, clone MIB, DAKO) at 4 °C overnight. Extensive rinsing was conducted before and after incubation with secondary antibody (donkey anti mouse IgG-Alexa 488 and donkey anti rabbit IgG-Alexa 555, Molecular probe) for 1 h at room temperature. DNA was counterstained with ToPro-3 iodide (Molecular probe) and slides mounted with ProLongGold (Molecular Probe).

For every xenograft, four consecutive images were taken into the tumour starting at the capsule. Vascularization for each image was measured as the ratio between the area stained with CD31 and the area stained with ToPro-3 iodide (DNA). Cell proliferation was measured in each image as the mean intensity of Ki67 signal in areas staining for ToPro-3 iodide (DNA).

Fluorescence images were obtained with a Zeiss LSM 510-inverted confocal microscope using a planapochromat 20× numerical aperture (NA) 0.75 objective.

**Patient-derived xenograft.** A 65-year-old male patient with BRAF<sup>V600E</sup> mutated metastases from an unknown primary melanoma was initially treated with carboplatin/DTIC. After disease progression, the patient was included in a clinical trial and received vemurafenib (BRAF<sup>V600E</sup> inhibitor), a treatment that was later stopped due to tumour progression and toxicity. The patient subsequently underwent a subacute surgical resection of a bulky small bowel mesentery metastasis with fistulation. The patient's post-operative course was uncomplicated, but was followed by the development of lethal brain metastases. After informed consent and approval from the regional ethics committee in Gothenburg (#288-12), material from the resected metastasis was dispersed using a Tissue Chopper (McIlwain) down to 1 µm large pieces. After filtration through a 70 µm cell strainer, cells were pelleted by centrifugation and dissolved in RPMI1640 medium and mixed with an equal volume of Matrigel. The suspension was injected subcutaneously into the flank of a NOD-SCID IL2Rγ<sup>null</sup> (NOG) mouse, creating the first passage patient-derived xenograft. When the tumour had grown to 200 mm<sup>3</sup>, the mouse was killed. The tumour was excised, dispersed and serially transplanted into three new NOG mice. The tumour that first reached the size of 200 mm<sup>3</sup> was further transplanted into ten mice (NOG mice, female, 8–12 weeks, Taconic). When these new tumours had reached a size between 50–100 mm<sup>3</sup>, the mice were randomized into two treatment groups receiving daily subcutaneous injections of either 30 mg kg<sup>-1</sup> TH588 or vehicle (10% *N*-methylpyrrolidone, 90% PEG300). Tumour sizes were measured once weekly by calipers. The animal experiments were performed in accordance with the regional animal ethics committee approval (#289-11).

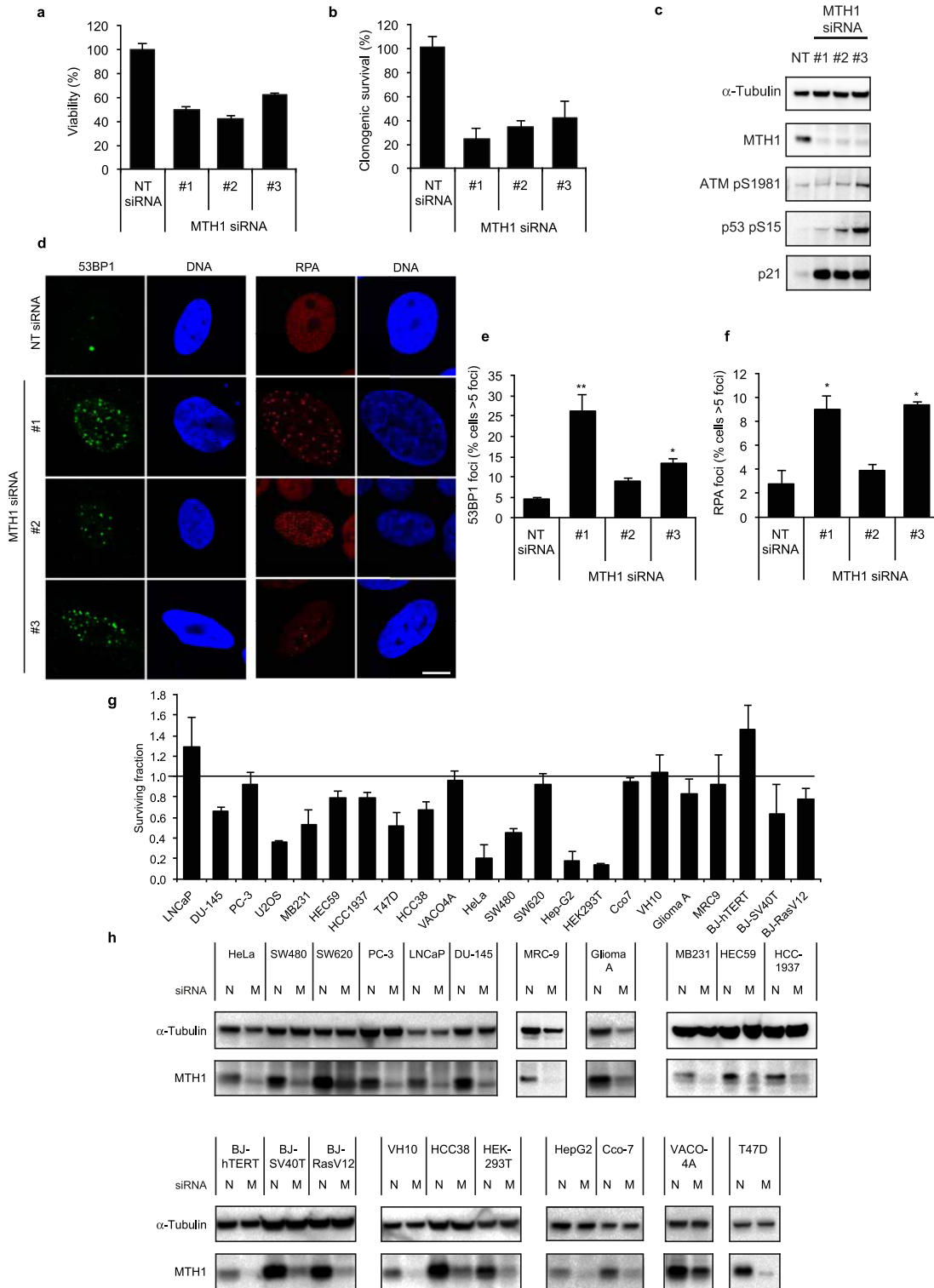
**Bioanalysis of samples from pharmacokinetic studies.** The target compound and its metabolite were dissolved in mouse EDTA plasma (Equitech-Bio, Inc) to give a stock standard solution with a concentration of 50 µM. Seven standard concentrations (0.5, 0.75, 1.5, 3, 5, 7.5, 10 µM) were used for the standard curve and calculations were performed using linear regression. For assessment of precision and accuracy, control samples at three different concentration levels (low, 1 µM; middle, 4 µM; and high, 8 µM) in replicates of five were prepared from the stock standard solution by dilution with mouse blood plasma. Selectivity test was performed by screening pooled blank mouse plasma from a number of individuals. Carry-over effect was evaluated for concentrations of 10 and 50 µM.

Analysis of samples from PK studies on mouse was performed by using 20 µl plasma sample aliquots to which the internal standard (6-(3-chlorophenyl)-*N*-methylpyrimidine-2,4-diamine), dissolved in 2% formic acid (HPLC grade, Rathburn) in water, was added (20 µl, 5 µM). After ultrasonication for 5 min acetonitrile (HPLC grade, Rathburn) was added (200 µl) to precipitate plasma proteins and the sample was centrifuged for 5 min at 10,000 r.p.m. The supernatant (150 µl) was evaporated in Speed Vac (Savant, SPD111V) and reconstituted in 150 µl 5% acetonitrile containing 0.1% formic acid. A 50 µl sample aliquot was injected onto the column.

**LC-MS method for bioanalysis of samples from pharmacokinetic studies.** The bioanalysis was performed using Shimadzu pumps coupled to a Sciex API2000 triple quadrupole mass spectrometer. The compounds were separated on a XBridge C18 column (2.1 × 7.5 mm, 2.5 µm, Waters) at a flow rate of 300 µl min<sup>-1</sup> by gradient elution. Mobile phase A was comprised of 0.1% formic acid in water, and mobile phase B consisted of 0.1% formic acid in acetonitrile. The gradient was run starting from 5% to 100% mobile phase B in 10 min. The mass spectrometer was operated in positive electrospray ionization mode using multiple reaction monitoring scan type. Scan speed was set to 100 ms per transition. Ionization spray voltage was set to 4 kV and temperature was maintained at 350 °C. Gas flow rates were adjusted to the mobile phase flow rate and composition (gas 1 and 2, 60). For each compound two transitions were monitored, where the first was used for quantification and the second was used for identity confirmation: TH287 (*m/z* 269 > 252 and *m/z* 269 > 227; declustering potential, 35; collisional energy, 40), TH588 (*m/z* 295 > 268; DP, 60; CE, 50 and *m/z* 295 > 279; DP 60, CE, 40), metabolite (*m/z* 255 > 213 and *m/z* 255 > 238; DP, 70; CE, 30) and internal standard (*m/z* 235 > 218; DP, 70; CE, 35 and *m/z* 235 > 193; DP, 70; CE, 35).

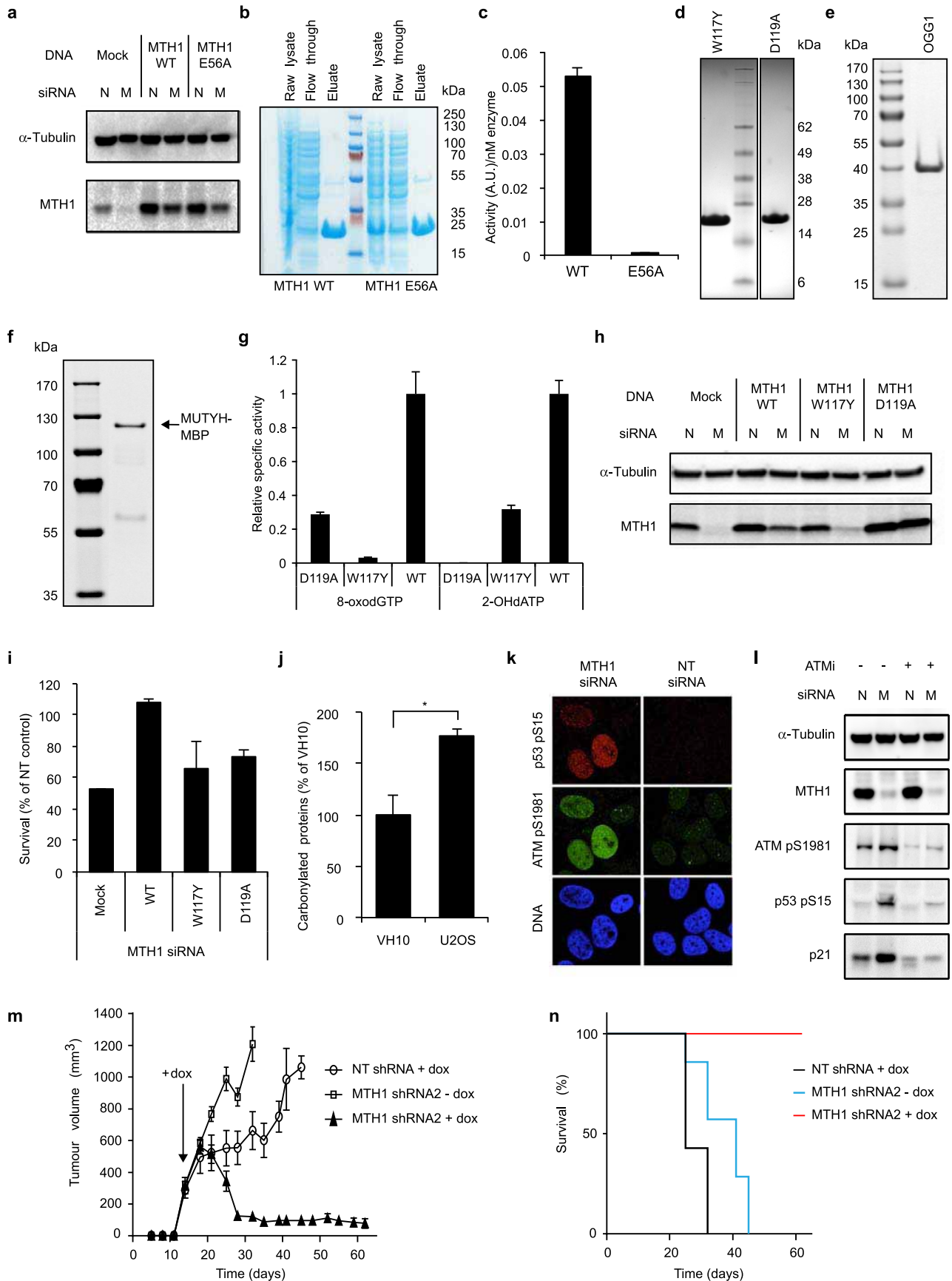
32. Mohindra, A. et al. Defects in homologous recombination repair in mismatch-repair-deficient tumour cell lines. *Hum. Mol. Genet.* **11**, 2189–2200 (2002).
33. Rai, P. et al. Continuous elimination of oxidized nucleotides is necessary to prevent rapid onset of cellular senescence. *Proc. Natl Acad. Sci. USA* **106**, 169–174 (2009).
34. Herold, M. J., van den Brandt, J., Seibler, J. & Reichardt, H. M. Inducible and reversible gene silencing by stable integration of an shRNA-encoding lentivirus in transgenic rats. *Proc. Natl Acad. Sci. USA* **105**, 18507–18512 (2008).
35. O'Brien, J., Wilson, I., Orton, T. & Pognan, F. Investigation of the Alamar Blue (resazurin) fluorescent dye for the assessment of mammalian cell cytotoxicity. *Eur. J. Biochem.* **267**, 5421–5426 (2000).
36. Struthers, L., Patel, R., Clark, J. & Thomas, S. Direct detection of 8-oxodeoxyguanosine and 8-oxoguanine by avidin and its analogues. *Anal. Biochem.* **255**, 20–31 (1998).
37. Dalle-Donne, I., Rossi, R., Giustarini, D., Milzani, A. & Colombo, R. Protein carbonyl groups as biomarkers of oxidative stress. *Clin. Chim. Acta* **329**, 23–38 (2003).

38. Baykov, A. A., Evtushenko, O. A. & Awaeva, S. M. A malachite green procedure for orthophosphate determination and its use in alkaline phosphatase-based enzyme immunoassay. *Anal. Biochem.* **171**, 266–270 (1988).
39. Britsun, V. M. & Maiboroda, E. I. Cyclocondensations of 3-(R2-amino)-3-methylthio-1-R1-propenones with 2-aminoazoles. *Ukr. Khim. Zh.* **74**, 126–128 (2008).
40. Kabsch, W. Xds. *Acta Crystallogr. D* **66**, 125–132 (2010).
41. Murshudov, G. N., Vagin, A. A. & Dodson, E. J. Refinement of macromolecular structures by the maximum-likelihood method. *Acta Crystallogr. D* **53**, 240–255 (1997).
42. Emsley, P. & Cowtan, K. Coot: model-building tools for molecular graphics. *Acta Crystallogr. D* **60**, 2126–2132 (2004).
43. Waters, N. J., Jones, R., Williams, G. & Sohal, B. Validation of a rapid equilibrium dialysis approach for the measurement of plasma protein binding. *J. Pharm. Sci.* **97**, 4586–4595 (2008).
44. Houston, J. B. Utility of in vitro drug metabolism data in predicting in vivo metabolic clearance. *Biochem. Pharmacol.* **47**, 1469–1479 (1994).
45. Baranczewski, P. et al. Introduction to in vitro estimation of metabolic stability and drug interactions of new chemical entities in drug discovery and development. *Pharmacol. Rep.* **58**, 453–472 (2006).
46. Hubatsch, I., Ragnarsson, E. G. & Artursson, P. Determination of drug permeability and prediction of drug absorption in Caco-2 monolayers. *Nature Protocols* **2**, 2111–2119 (2007).



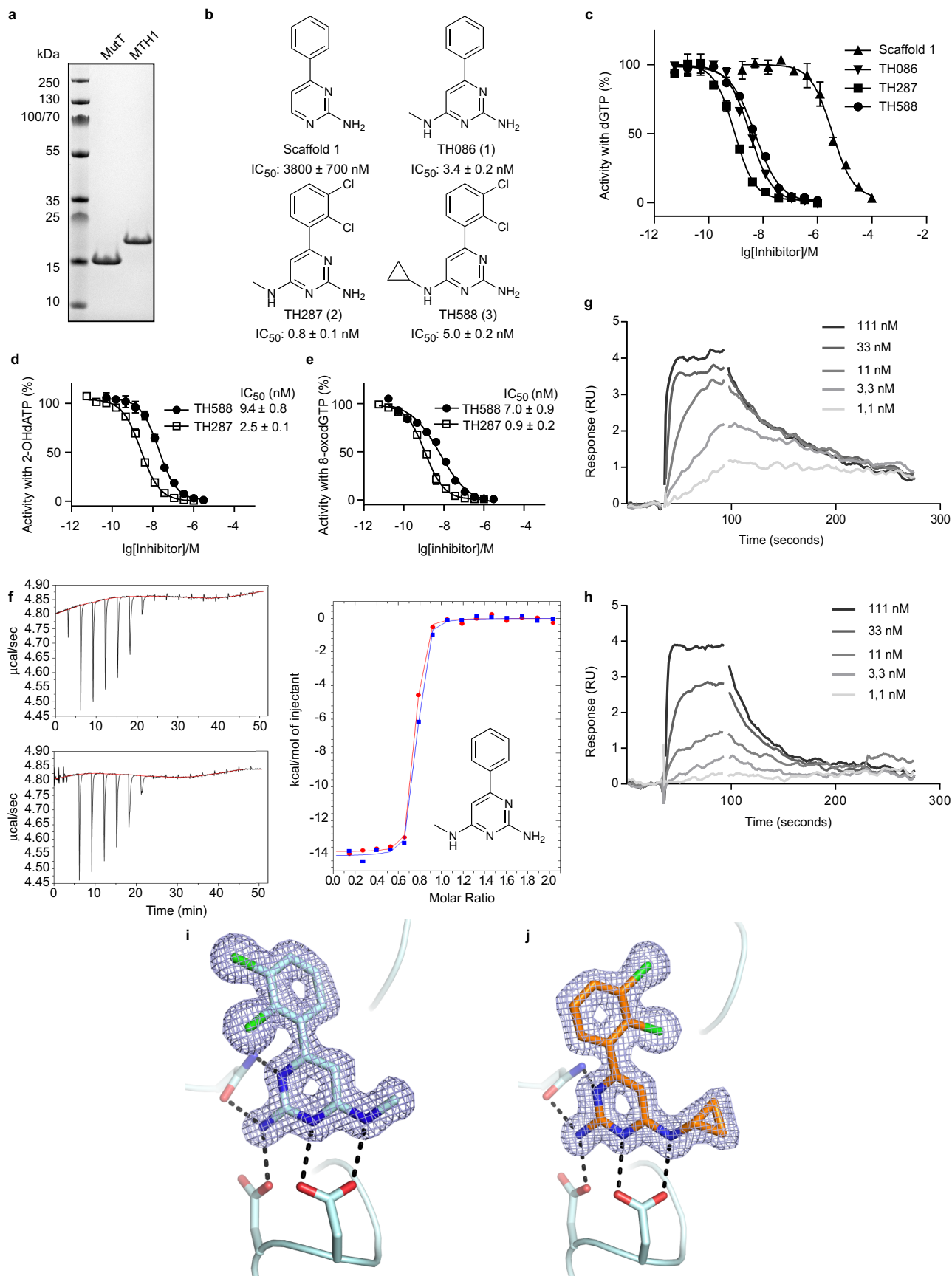
**Extended Data Figure 1 | Transient siRNA depletion of MTH1 reduces cell survival and causes DNA damage.** **a–d**, U2OS cells were transfected with siRNA for 3 days, after which **(a)** cell viability was determined after additional 3 days in culture; **(b)** cells were trypsinized, counted and re-seeded for clonogenic outgrowth; **(c)** proteins extracted and analysed with western blot (data shown as average  $\pm$  s.d. from three independent experiments for **a–c**); or **(d)** grown for additional 3 days and immunoblotted with 53BP1 and RPA-32 antibodies and analysed with immunofluorescence. DNA was counterstained with ToPro-3 iodide. **e, f**, Quantification of 53BP1 **(e)** (data shown as average  $\pm$  s.e.m. from three independent experiments,  $*P < 0.05$ ;  $**P < 0.01$ , one-way ANOVA) and RPA foci **(f)** (percentage of cells  $>5$  foci per cell) after

*MTH1* siRNA transfection. Data shown as average  $\pm$  s.e.m. from two experiments.  $*P < 0.05$ , one-way ANOVA. **g**, Transient siRNA depletion of MTH1 reduces cell survival to various extents in cancer cell lines. Indicated cells were transfected with *MTH1* siRNA #3 (M) and non-targeting control (N) for 3 days. The cells were trypsinized, counted and re-seeded for clonogenic outgrowth. Values represent relative survival of *MTH1* siRNA-transfected cells compared to non-targeting control. Data shown as average  $\pm$  s.d. from two independent experiments. **h**, The cells were collected, proteins extracted and analysed with western blot. Figure shows one representative western blot from two independent experiments. MTH1 knockdown by siRNA induces cell death in most cancer cells, but not in normal cells (VH10, MRC-9, BJ-hTERT).



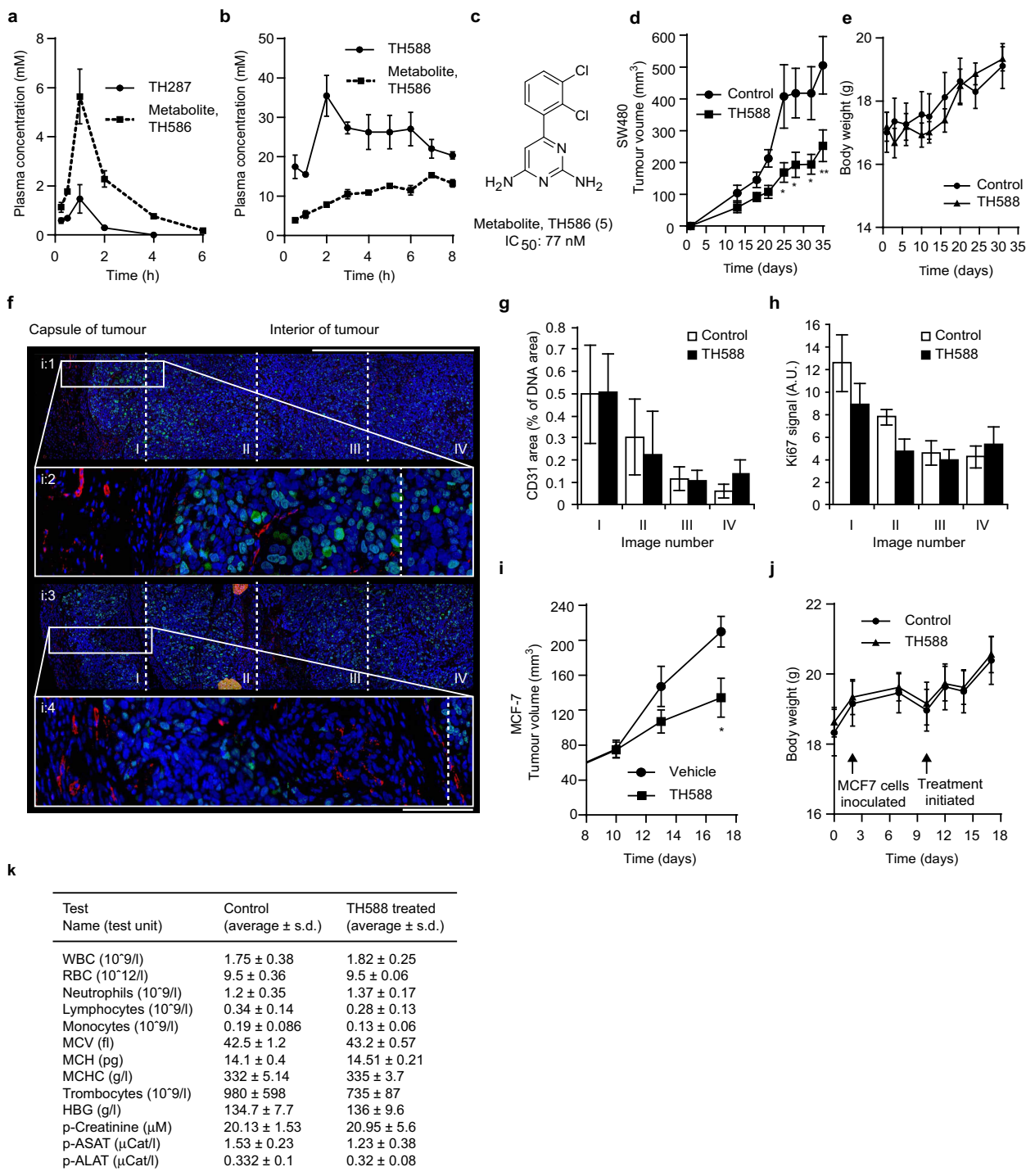
**Extended Data Figure 2 | Rescue expression of RNAi-resistant wild-type MTH1 and catalytically dead MTH1(E56A) mutant and purification of MTH1 protein and activity measurements.** **a**, U2OS cells stably overexpressing RNAi-resistant wild-type (WT) MTH1 and catalytically dead mutant (E56A) were transfected for 72 h, and western blot of MTH1 protein levels in non-targeting siRNA (N), *MTH1* siRNA (M), *MTH1* wild type (WT) or MTH1 E56A is shown. Figure shows one representative western blot from three independent experiments. **b**, The MTH1 wild type (WT) or MTH1 E56A were expressed in *E. coli* and purified to >98% purity. **c**, Relative activity of MTH1 wild type and E56A catalysed hydrolysis of dGTP, demonstrating that the E56A is a catalytically dead mutant of MTH1. Data shown as a representative graph, average  $\pm$  s.d. from two independent experiments, each performed in triplicate. **d–f**, SDS–PAGE gels showing (**d**) the purity of the MTH1 W117Y and D119A mutant proteins; (**e**) the purity of expressed and purified OGG1; and (**f**) the purity of expressed and purified MUTYH in fusion with MBP (maltose binding protein). **g**, Activity of MTH1 mutants D119A and W117Y relative to wild type with 20  $\mu$ M 8-oxodGTP and 2-OHdATP. Data shown as average  $\pm$  s.d. from two independent experiments, each performed in triplicates. **h**, U2OS cells stably overexpressing RNAi-resistant wild-type MTH1 and MTH1 mutants (D119A and W117Y) were transfected for 72 h and western blot of MTH1 protein levels in non-targeting siRNA (N) and *MTH1* siRNA (M) is shown. Figure shows one representative western blot from two

independent experiments. **i**, Clonogenic survival of U2OS cells transiently transfected with *MTH1* siRNA (M) or NT siRNA (N). Cells were transfected for 72 h and reseeded for clonogenic outgrowth. Values represent average  $\pm$  s.d. from two independent experiments. **j**, Determination of carbonylated proteins in primary VH10 and U2OS cancer cells. Values represent average  $\pm$  s.e.m. from four independent experiments. Statistically significant  $P = 0.033$  in Student's *t*-test. **k**, Immunofluorescent staining of phospho-p53 (S15) and phospho-ATM (S1981) in U2OS cells transiently transfected with NT siRNA or *MTH1* siRNA. **l**, ATM phosphorylation, p53 phosphorylation and p21 induction is induced by *MTH1* siRNA depletion (M) in U2OS cells, but not in NT siRNA control (N). Incubation with ATM inhibitor KU55933 (10  $\mu$ M) prevents ATM and p53 phosphorylation after *MTH1* siRNA depletion as well as induction of p21. **m**, The second independent experiment using *MTH1* shRNA as in Fig. 2l. Doxycycline was added to the drinking water (indicated by the arrow) ( $n = 7$  per group, data shown as average  $\pm$  s.e.m.). **n**, Kaplan–Meyer survival plot of mice carrying SW480 tumours with the indicated construct and addition of doxycycline to the drinking water. At a volume size of 1,000 mm<sup>3</sup>, animals were euthanized. All animals in the control groups, *MTH1* shRNA without doxycycline and NT shRNA with doxycycline, had reached the upper limit of tumour size at 45 and 32 days, respectively, whereas the *MTH1* shRNA knockdown group was all still alive at day 62.



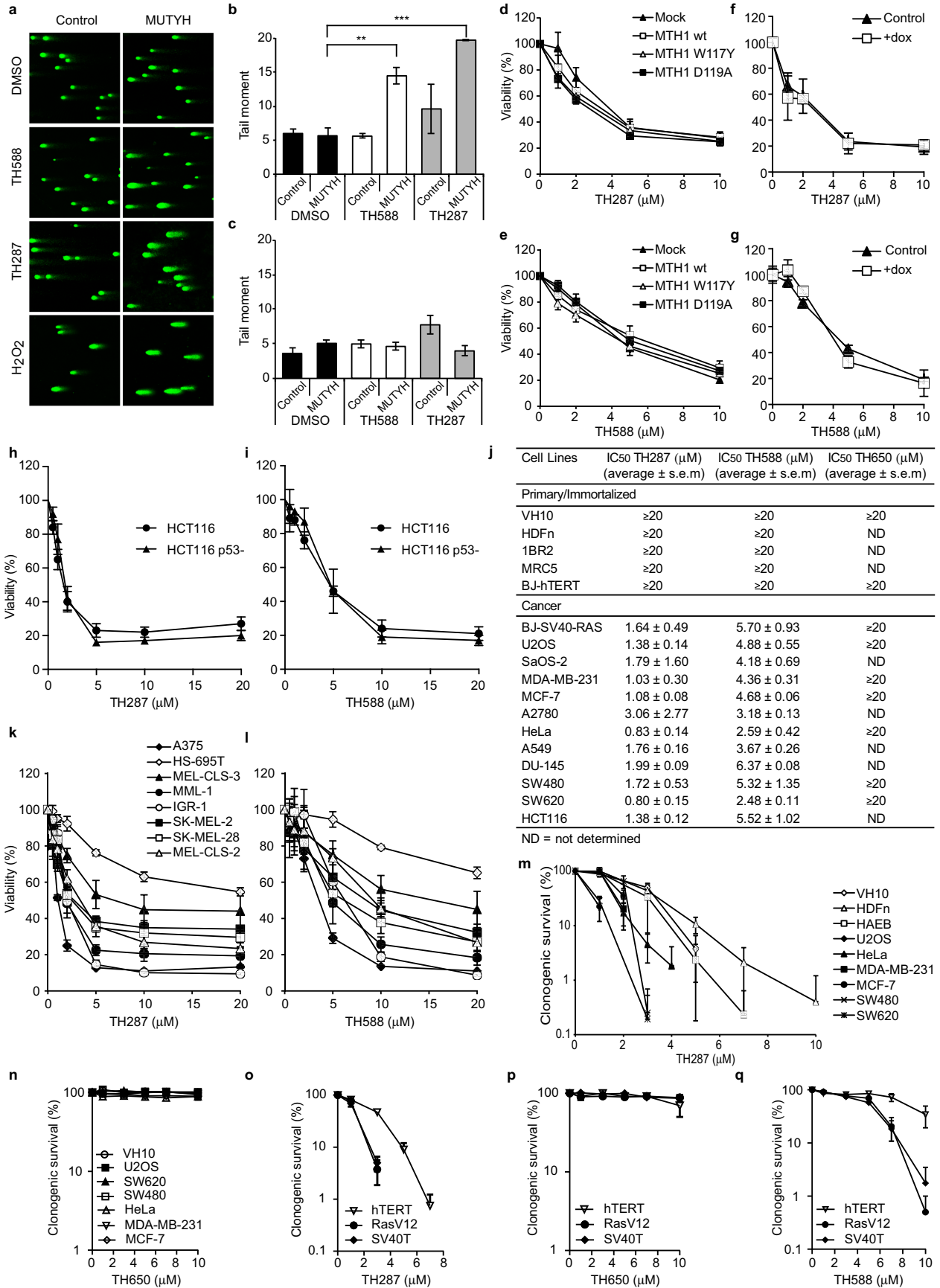
**Extended Data Figure 3 | Screening for MTH1 inhibitors and MTH1 protein binding.** **a**, Purity of MTH1 and MutT preparations used. **b**, High-throughput screening identified hits containing 2-aminopyrimidine motif (scaffold 1). By introducing an aminomethyl substituent a marked increase in potency was observed (TH086). The dichlorophenyl derivative TH287 showed further improved potency, however, with a high intrinsic clearance in mouse liver microsomes. The cyclopropyl compound TH588 displayed increased metabolic stability while retaining potency against MTH1. ( $IC_{50}$  values, determined using the sensitive version of the malachite-green-based enzymatic assay, are displayed as average  $\pm$  s.d.,  $n = 3$  independent experiments.) **c**, Representative dose-response curves of scaffold 1, TH086, TH287 and TH588. **d**, **e**, 2-OHdATP (**d**) or 8-oxodGTP (**e**) was used as substrates showing that the inhibition of MTH1 by TH588 and TH287 is substrate independent. (Graphs in **c**, **d** and **e** show representative curves, average  $\pm$  s.d. from two replicates;  $IC_{50}$  values were determined using the PPILight Inorganic Pyrophosphate Assay kit (Lonza) and are presented as average  $\pm$  s.d. from two independent experiments.) **f**, To confirm binding of optimized hits to MTH1

protein, ITC experiments were performed. Left-hand graphs show raw data (black) from two independent titrations of TH086 (129  $\mu$ M) into a solution containing MTH1 protein (30  $\mu$ M). The right-hand graph shows the integrated heats from the titrations of TH086 into a solution containing MTH1 as a function of their molar ratio. The solid lines represent the best-fit binding isotherms to the data (one set of sites model within the Origin software),  $K = 6.1 \pm 1.5 \times 10^7 \text{ M}^{-1}$ ,  $\Delta H = -59 \pm 0.5 \text{ kJ per mole}$  and  $n = 0.71$  (blue) and  $K = 9.2 \pm 2.2 \times 10^7 \text{ M}^{-1}$ ,  $\Delta H = -58 \pm 0.4 \text{ kJ per mole}$  and  $n = 0.70$  (red), respectively. **g**, **h**, Biacore surface plasmon resonance technique was used to determine the affinity of (**g**) TH287 (average  $\pm$  s.d.:  $K_d = 1.7 \pm 0.6 \text{ nM}$ ,  $n = 3$ ) and (**h**) TH588 (average  $\pm$  s.d.;  $K_d = 15.5 \pm 2.9 \text{ nM}$ ,  $n = 3$ ) to the MTH1 protein. Representative sensorgram for each inhibitor is shown ( $n = 3$  independent experiments). Data points confounded by the buffer change during the start and end of injection are excluded from the analysis and the graphic representation. **i**, **j**, Electron density for (**i**) TH287 and (**j**) TH588.  $2F_o - F_c$  maps contoured at  $1.5\sigma$ .



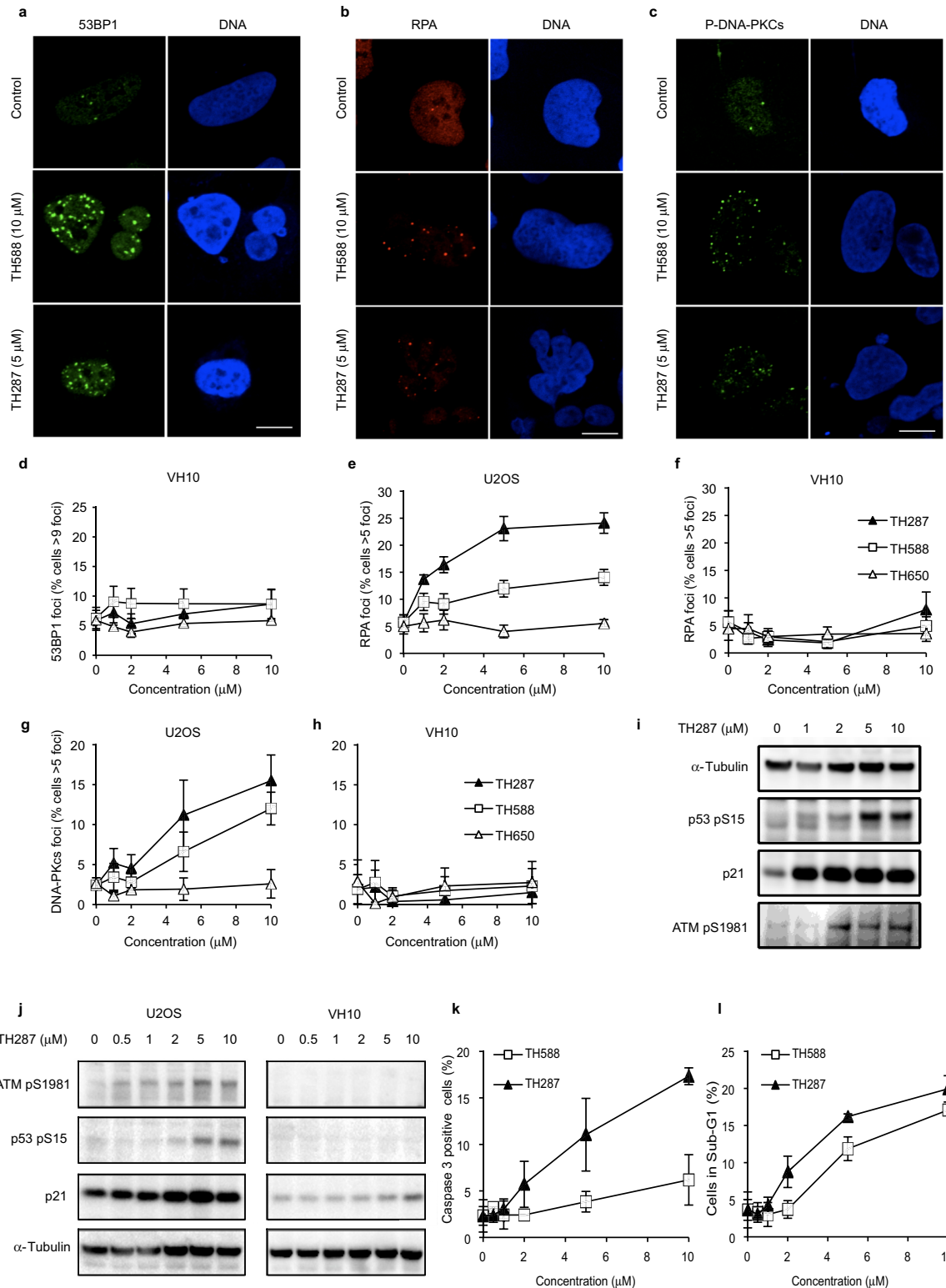
**Extended Data Figure 4 | TH588 reduces tumour growth in mouse xenografts.** **a**, Pharmacokinetic profiles of TH287 (10 mg kg<sup>-1</sup>, s.c.). **b**, TH588 pharmacokinetic profile (30 mg kg<sup>-1</sup>, s.c.) (average  $\pm$  s.e.m. ( $n = 3$  per data point) in **a**, **b**). (See also Extended Data Table 2.) **c**, Chemical structure and  $IC_{50}$  value of TH287's and TH588's major metabolite TH586. **d**, **e**, TH588 (30 mg kg<sup>-1</sup> s.c., once daily (q.d.)) significantly reduced tumour growth in SW480 xenograft mice after 35 days treatment (average  $\pm$  s.e.m.,  $n = 8$  per group, two-way ANOVA with repeated measures; \* $P < 0.05$ , \*\* $P < 0.01$ ) (**d**), with no effect on body weight (**e**). **f**, Tiled images of SW480 xenograft with start at the capsule (left) of the tumours. Green stain shows Ki67, red stain shows CD31, blue stain shows DNA signal. Scale bar, 1 mm. i:1, untreated xenograft; i:2, xenograft treated with TH588. i:3 and i:4 show close-ups of the marked area in i:1 and i:2. Scale bar, 100  $\mu$ m. **g**, **h**, Vascularization (CD31), measured as the area of CD31 staining normalized against area of DNA (**g**), and

proliferation (Ki67), measured as the mean signal of Ki67 in areas with DNA (**h**), in untreated and TH588-treated xenograft in relation to the distance from the capsule of the tumours (average  $\pm$  s.e.m. untreated,  $n = 7$  for TH588 treated,  $n = 8$  for untreated **g**, **h**). **i**, **j**, TH588 (30 mg kg<sup>-1</sup> s.c., q.d) significantly reduced tumour growth in MCF-7 xenograft (**i**) (average  $\pm$  s.e.m.,  $n = 10$  per group, two-way ANOVA with repeated measures; \* $P < 0.05$ ) with no effect on body weight (**j**). **k**, Clinical parameters measured in blood from SW480 xenograft animals in **d**, **e**. The mean values of white blood cells (WBC), red blood cells (RBC), neutrophils, lymphocytes, monocytes, mean corpuscular volume (MCV), mean cell haemoglobin (MCH), mean cell haemoglobin concentration (MCHC) from the different groups are presented in the table. The results did not show any significant differences in the haematology parameters or the liver/heart/kidney parameters between control and treated groups.



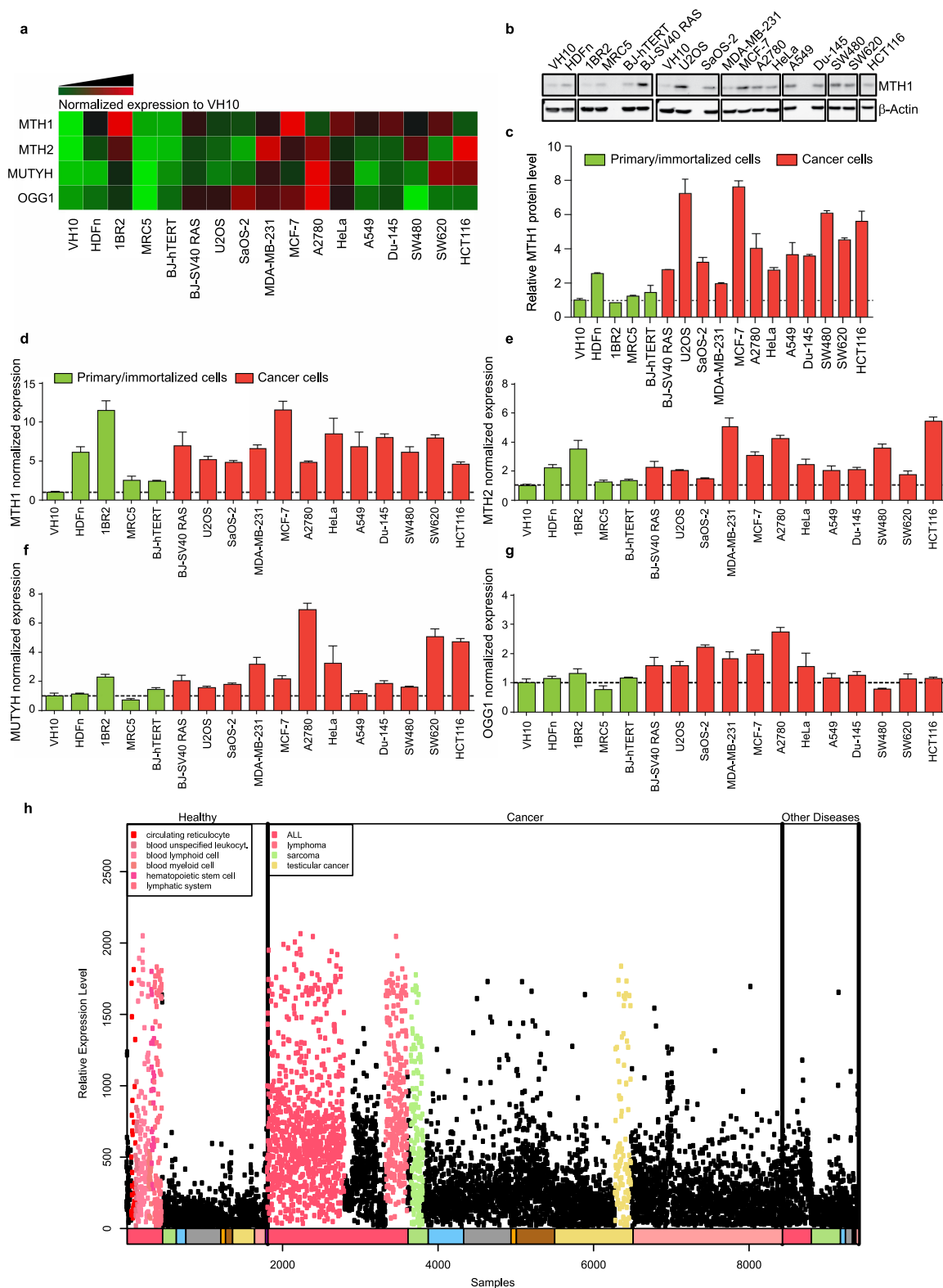
**Extended Data Figure 5 | MTH1 inhibitors TH588 and TH287 induce oxidative lesions in the DNA and kill cancer cells.** **a–c**, U2OS cells (**a**, **b**) or VH10 cells (**c**) were treated with 10  $\mu$ M MTH1 inhibitor for 24 h before being incubated with MUTYH or with buffer alone (control) and run in alkaline comet assay. As a positive control, cells were treated with 100  $\mu$ M H<sub>2</sub>O<sub>2</sub> for 5 min on ice. Tail moment is calculated as per cent DNA in the tail multiplied by the tail length. Values represent average  $\pm$  s.e.m. from three experiments; \* $P < 0.05$ ; \*\* $P < 0.01$ ; \*\*\* $P < 0.001$ , one-way ANOVA. **d**, **e**, Viability determined by resazurin in U2OS cells expressing wild-type MTH1, MTH1(W117Y) or MTH1(D119A) exposed 72 h to increasing concentrations of MTH1 inhibitors (**d**) TH287 or (**e**) TH588. Data are shown as average  $\pm$  s.e.m. from three independent experiments. **f**, **g**, Viability of U2OS cells stably carrying doxycycline-inducible p53 shRNA constructs after 72 h exposure to different concentrations of MTH1 inhibitors (**f**) TH287 or (**g**) TH588. Data shown as average  $\pm$  s.e.m. from two independent experiments. **h**, **i**, Viability of HCT116 and HCT116 *p53*<sup>-/-</sup> after 72 h exposure to different concentrations of MTH1 inhibitors (**h**) TH287 or (**i**) TH588. Values represent percentage of cells in relation to mock-treated controls displayed as average  $\pm$  s.d. from three independent experiments. **j**, Cell viability after MTH1 inhibitor treatment determined by resazurin assay in primary or

immortalized cells or in cancer cell lines. All data are average  $\pm$  s.e.m. of at least three independent experiments. ND, not determined. **k**, **l**, Viability determined in melanoma cancer cell lines after exposure for 72 h to increasing concentrations of MTH1 inhibitors (**k**) TH287 or (**l**) TH588. Values represent percentage of cells in relation to mock-treated controls displayed as mean  $\pm$  s.d. from three independent experiments, each done in duplicate. **m**, Effect of TH287 on clonogenic cell survival in primary or immortalized cells (open) or in cancer cell lines (filled). **n**, No toxicity was observed in clonogenic survival of TH650 in various cell lines. **o–q**, Clonogenic survival of BJ cells after treatment with (**o**) TH588, (**p**) TH287, and (**q**) TH650. TH588 and TH287 both significantly reduce cell survival primarily in hTERT immortalized BJ cells transfected with SV40 large T (Sv40T) or SV40 large T and Ras (RasV12), whereas no toxicity was observed with the less potent MTH1 inhibitor TH650. For **m–q**: cells were seeded in 6-well plates (200 cells per well for primary/immortalized cells, except BJ-hTERT) or in 10-cm dishes (500 cells per dish for all other cells) in triplicates and the day after treated with 0–10  $\mu$ M compound for 7–10 days after which the number of colonies were counted. Values represent percentage of colonies in relation to DMSO-treated controls displayed as average  $\pm$  s.d. from three independent experiments.



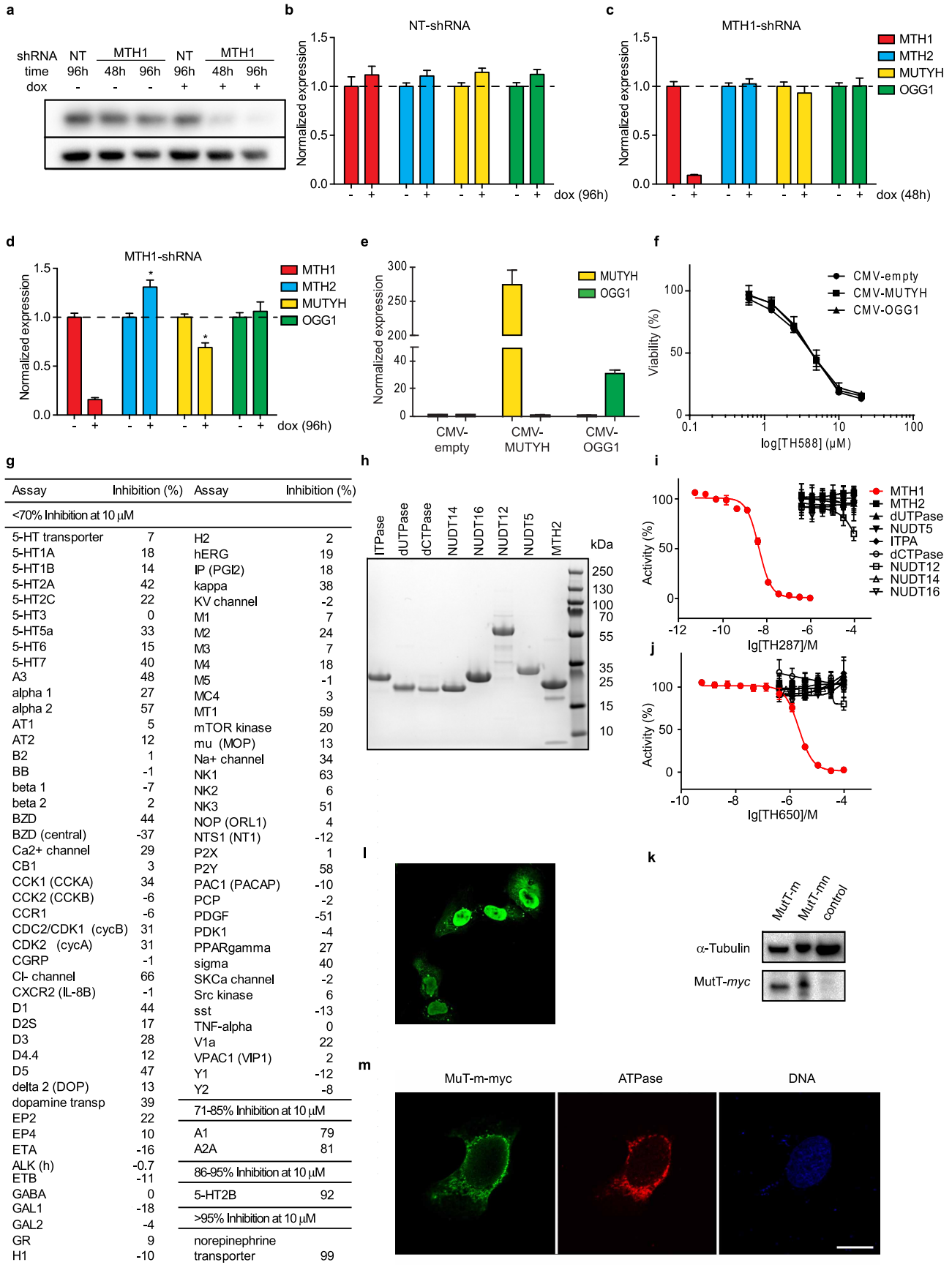
**Extended Data Figure 6 | MTH1 inhibitors induce DNA damage foci in U2OS but not in VH10 cells.** **a–l**, Cells were seeded on coverslips (**a–c**), 96-well plates (**d–h**) or 6-well plates (**i–l**) and were the following day treated with TH287, TH588 and TH650. DMSO concentration was kept constant. **a–h**, Samples were fixed with formaldehyde after an additional 72 h and immunostained with (**a, d**) 53BP1, (**b–f**) RPA and (**c, g, h**) DNA-PKcs pS2056 antibodies followed by secondary Alexa-conjugated antibodies. The DNA was counterstained with (**a–c**) To-Pro3 or (**d–h**) DAPI. Images were acquired and the number of foci was quantified by automatic image analysis. Scale bar, 10  $\mu$ m. Data shown as average  $\pm$  s.e.m. from three (**d, g, h**) or four

(**e, f**) independent experiments. **i–l**, Cells were washed with PBS and detached by scraping in lysis buffer. **i, j**, Samples were analysed on western blot with ATM phospho-S1981, p53 phospho-S15, p21 and  $\alpha$ -tubulin antibodies. **k, l**, FACS analysis of apoptosis in U2OS cells treated with TH287 and TH588 for 72 h. **k**, Quantification of the percentage of cleaved caspase 3 positive cells. **l**, Propidium iodine staining and quantification of percentage of cells in sub-G1 phase. Data shown as average  $\pm$  s.e.m. from two independent experiments performed in duplicate. Blots shown as a representative blot from two experiments.



**Extended Data Figure 7 | Expression level of MTH1, MTH2, MUTYH or OGG1 in cell lines used in this study.** **a**, Heat-map diagram of MTH1, MTH2, MUTYH and OGG1 gene expression determined by qRT-PCR in the same cell lines. The expression levels are normalized to VH10 cells.  $\Delta\Delta Cq$  value was calculated using Bio-Rad CFX Manager 3. The normalized values below 1 have lighter green colour than VH10. **b**, MTH1 protein levels determined by western blot analysis of cell lines used in this study. **c**, Quantification of MTH1 protein levels depicted as MTH1/actin ratio and normalized to VH10 cells, in primary

or immortalized cells (green) or in cancer cells (red) reveals no obvious correlation between protein levels and sensitivity to MTH1 inhibitors or siRNA response. Values represent average  $\pm$  s.d. from two experiments, except for cell line 1BR2 for which values represent one experiment. **d-g**, The bar chart display of panel **a**. Values represent average  $\pm$  s.e.m. from two experiments performed in triplicate. **h**, MTH1 (NUDT1) expression in normal and cancer tissues (from <http://www.genesapiens.org>).



**Extended Data Figure 8 | Expression analysis, MTH1 inhibitor selectivity and MutT overexpression.** **a**, Expression level of MTH1 after doxycycline-induced depletion in SW480 cells with MTH1 shRNA construct.

**b–d**, Quantification of MTH2 (NUDT15), MUTYH or OGG1 expression levels using qRT-PCR in **(b)** non-targeting (NT) shRNA, or doxycycline treatment for 48 h **(c)** or 96 h **(d)**. Values represent average  $\pm$  s.e.m. from three experiments performed in triplicate.  $\Delta\Delta Cq$  value was calculated using Bio-Rad CFX Manager 3. The expression levels were normalized to VH10 cells.

**e**, Overexpression of OGG1 or MUTYH in U2OS cells determined by qRT-PCR expression. Values represent average  $\pm$  s.e.m. from two independent experiments, each performed in triplicate.  $\Delta\Delta Cq$  value was calculated using Bio-Rad CFX Manager 3. The expressions were normalized to the CMV-empty control. \* $P < 0.05$ , Student's *t*-test by Bio-Rad CFX manager 3. **f**, Survival in U2OS overexpressing either MUTYH or OGG1 after 72 h treatment with TH588. Values represent average  $\pm$  s.d. from three independent experiments, each performed in triplicate. **g**, Selectivity of TH588 against a panel of diverse GPCRs, ion channels, transporters and enzymes, including ALK kinase. TH588 (10  $\mu$ M) was tested at CEREP high-throughput screening panel to obtain

information about possible cross-reactivity. Notably, TH588 did not show any significant inhibitory effect on hERG. Additional functional studies need to be performed before a full evaluation of selectivity of the compound can be made.

**h**, Purity of enzyme preparations used in the selectivity screen. 4  $\mu$ g of the enzyme preparations used were analysed using SDS-PAGE followed by Coomassie staining. **i**, Inhibition analysis of TH287 showing >1,000 fold selectivity for MTH1. Data shown as average  $\pm$  s.d.,  $n = 3-6$  independent experiments performed in duplicate. **j**, Inhibition analysis of TH650 showing >100 fold selectivity for MTH1. Data shown as average  $\pm$  s.d.,  $n = 3-6$  independent experiments performed in duplicate. **k**, MutT overexpression in U2OS cells. Western blot of U2OS cells stably transfected with MutT-MLS-*myc* (MutT-m), MutT-*myc* + MutT-MLS-*myc* (MutT-mn) or no expression (control) immunoblotted with *Myc* and tubulin antibodies. **l**, Immunofluorescence image of U2OS cells transiently transfected with MutT-mn and immunostained with *Myc* antibody. **m**, Immunofluorescence image of U2OS cells transiently transfected with MutT-m and immunostained with *Myc* and ATP synthase antibodies followed by secondary Alexa-conjugated antibody. DNA was counterstained with To-Pro3. Scale bar, 20  $\mu$ m.

Extended Data Table 1 | Data collection and refinement statistics for MTH1 + TH287 and MTH1 + TH588 co-crystal structure

Data collection	TH287	TH588
Space group	P2 <sub>1</sub> 2 <sub>1</sub> 2	P2 <sub>1</sub> 2 <sub>1</sub> 1
a, b, c (Å)	60.4, 66.3, 36.1	57.7, 66.1, 72.5
$\alpha$ , $\beta$ , $\gamma$ (°)	90, 90, 90	90, 90, 90
Resolution (Å)	44.7 – 1.6 (1.7 – 1.6)	48.8 – 1.6 (1.68 – 1.6)
R <sub>meas</sub> (%)	5.7 (44.5)	7.8 (70.3)
I/ $\sigma$ (I)	20.3 (3.8)	17.4 (2.7)
Completeness (%)	99.2 (97.2)	99.8 (98.8)
Redundancy	4.7 (4.7)	6.5 (6.3)
Refinement		
Resolution (Å)	44.7 – 1.6	48.8 – 1.6
No. unique reflections	18699 (3115)	35596 (2528)
R <sub>work</sub> /R <sub>free</sub>	18.1 / 21.4	18.0 / 20.4
No. atoms		
Protein	1302	2581
Ligand	17	38
Water	139	218
B-factors		
Protein	16.0	18.9
Ligand	14.9	15.8
Water	31.4	32.4
R.m.s. deviations		
Bond lengths (Å)	0.011	0.011
Bond angles (°)	1.52	1.58
Ramachandran plot residues in (%)		
Most favourable region	99.3	99.0
Additional allowed region	0.7	1.0

Extended Data Table 2 | Summary of *in vitro* ADME properties of selected MTH1 inhibitor compounds

In vitro ADME properties										
Compound	Predicted phys-chem properties#			Solubility ( $\mu\text{M}$ )	PPB, fu (%)	CLint in MLM ( $\mu\text{L}/\text{mg}/\text{min}$ )	CLint in HLM ( $\mu\text{L}/\text{mg}/\text{min}$ )	Papp $\times 10^{-5}$		Efflux ratio
	LogD	LogP	pKa					A-B (s.d)	B-A (s.d)	
TH287	3.17	3.21	6.2	52	8.0	261	54	8.4 (0.7)	6.6 (1.3)	0.8
TH588	3.64	3.67	6.2	22	1.7	151	51	3.9 (0.4)	3.3 (1.1)	0.8
TH650	3.02	3.05	6.2	> 100	0.2	14	18	0.024 (0.0021)	0.043 (0073)	1.8

In vivo pharmacokinetic properties						
Parameter	TH287	TH586 metabolite	TH588	TH586 metabolite	TH588	TH586 metabolite
	single dose		single dose		3 days repeated dose	
Dose (mg/kg)	10	NA*	25	NA*	25	NA*
C <sub>max</sub> (M)	1.5	5.6	35	15	102	29
T <sub>max</sub> (h)	1	1	2	7	2	8
AUC 0 - t ( $\mu\text{mol} \cdot \text{h}/\text{mL}$ )	1.7	10.3	195	81	474	200
AUC 0 - inf ( $\mu\text{mol} \cdot \text{h}/\text{mL}$ )	1.8	10.5	337	174	488	205
$\lambda_z$ range (h)	1-2	4-6	7-8	-	8-24	8-12
t <sub>1/2 z</sub> (h)	0.4	1.0	4.8	ND**	6.1	1.2

fu, free fraction in plasma; HLM, human liver microsomes; MLM, mouse liver microsomes; PPB, plasma protein binding; s.d., standard deviation.

\*Not applicable.

\*\*Not determined.

# Physicochemical profiling was performed *in silico* using Marvin software (ChemAxon Kft).